

Redox-controlled chalcogen and pnictogen bonding: The case of a stibonium/sulfonium dication as a preanionophore for chloride anion transport

Gyeongjin Park and François P. Gabbaï*

Department of Chemistry, Texas A&M University, College Station, Texas 77843-3255, United States

SUPPORTING INFORMATION

This PDF file includes

Contents

Synthetic details	2
Computational details	27
Chloride anion binding experiments monitored by UV-vis spectroscopy in acetonitrile	40
Vesicle Preparation	45
Chloride efflux in the absence of valinomycin	46
Chloride efflux in the presence of valinomycin	46
Initial rate of chloride efflux in the presence of valinomycin	48
Hill plot measurements and analysis	53
Temperature-dependent chloride transport experiments in the presence of valinomycin using DPPC vesicles	56
Carboxylfluorescein (CF) non-specific leakage assay	57
Reduction of [4]²⁺ by DMSO or by GSH	59
Reduction of [4]²⁺ by GSH in DMSO:D₂O phosphate buffer (0.3 M, pH 7.6, v/v = 2.1:7.9)	61
GSH triggered activation of transport activity of [4]²⁺ in vesicles	62
References	63

Synthetic details

General Considerations. (2-bromophenyl)(phenyl)sulfane,¹ triphenylantimony dibromide,² tetraphenylstibonium tetrafluoroborate,³ tri-*p*-tolylantimony,⁴ tri-*p*-tolylantimony dibromide,² were prepared by following the literature. 1-Palmitoyl-2-oleoyl-*sn*-glycero-3-phosphocholine (POPC) and 1,2-dipalmitoyl-*sn*-glycero-3-phosphocholine (DPPC) were purchased from Avanti Polar Lipids. Valinomycin was purchased from BioWorld. Potassium gluconate, triphenylphosphine and phenylsulfide were purchased from TCI America. All commercially available compounds were used as received. The Mini-Extruder used for size selection of the vesicles was purchased from Avanti Polar Lipids. The Sephadex G-50 column was purchased from GE Healthcare – Life Sciences. Solvents were dried by refluxing under N₂ over Na/K or CaH₂ (Hexane, Et₂O, THF and DCM). All other solvents were ACS reagent grade and used as received. The synthesis of stibonium derivatives was carried out under a dry N₂ atmosphere with standard Schlenk techniques. ¹H, ¹³C, ³¹P, and ¹⁹F NMR spectra were recorded at room temperature on a Varian Inova 500 FT NMR spectrometer or a Bruker Avance II 400 spectrometer. Chemical shifts are given in ppm and are referenced to residual ¹H or ¹³C solvent signals. ISE assays were performed with an Oakton WD-35812-12 Chloride Double-junction Economy Epoxy Ion-Selective Electrodes connected to a pH-meter giving readings in mV (PHM 290, Meter lab, Radiometer Analytical S.A., Villeurbanne, Cedex, France). UV-vis titrations were performed using a Shimadzu UV-2502PC UV-Vis spectrophotometer.

Synthesis of *o*-PhS(C₆H₄)SbPh₃Br (1-Br): ⁿBuLi (2.4 mL, 6.17 mmol, 2.57 M in hexane) was added to a solution of (2-bromophenyl)(phenyl)sulfane (1.47 g, 5.54 mmol) in Et₂O at 0 °C. This solution was stirred for 3 hours at the same temperature, leading to the generation of *o*-PhS(C₆H₄)Li which was kept in solution. This solution was cooled to -78 °C before being subjected to the slow addition of a solution of triphenylantimony dibromide (2.8 g, 5.48 mmol) dissolved in a mixture of Et₂O (20 mL) and THF (20 mL). The resulting solution was warmed to room temperature and stirred overnight. The solvent was removed under vacuum and the residue extracted with dichloromethane (40 mL). The resulting solution was filtered through Celite and silica gel to remove LiBr. The filtrate was concentrated to a volume of 3 mL. Et₂O (30 mL) was then added, resulting in the formation of a white precipitate, which was removed by filtration. The filtrated solution was purified by chromatography over silica gel using hexane/ethyl acetate (1:1, v/v). Compound 1-Br, characterized by an R_f value is 5.5, was dried in vacuum and obtained as a white solid. Further washing with *n*-pentane (20 mL) and drying afforded 1.5 g of 1-Br (44% yield). Single crystals of 1-Br were obtained as colorless blocks by slow diffusion of hexanes into a CH₂Cl₂ solution of the compound. ¹H NMR (499 MHz, CDCl₃) δ 7.84 (d, *J* = 7.5 Hz, H), 7.62 (d, *J* = 7.1 Hz, 1H), 7.51 – 7.38 (m, 12H), 7.18 – 7.07 (m, 5H). ¹³C NMR (126 MHz, CDCl₃) δ 150.23 (s), 136.88 (s), 135.59 (s), 135.16 (s), 134.90 (s), 133.50 (s), 131.80 (s), 131.05 (s), 129.97 (s), 129.69 (s), 129.46 (s), 129.22 (s), 127.42 (s). ESI-MS calcd for C₃₀H₂₄SSb⁺ [M]⁺ 537.0631, found 537.0621.

Synthesis of *o*-PhS(C₆H₄)Sb(*p*-Tol)₃Br (2-Br): ⁿBuLi (1 mL, 2.5 mmol, 2.5 M in hexane) was added to a solution of (2-bromophenyl)(phenyl)sulfane (1.88 g, 5.54 mmol) in Et₂O (20 mL) at 0 °C. This solution was stirred for 3 hours at the same temperature, leading to the generation of *o*-PhS(C₆H₄)Li which was kept in solution. This solution was cooled to -78 °C before being subjected to the slow addition of a solution of tri-*p*-tolylantimony dibromide (1 g, 1.83 mmol)

dissolved in THF (10 mL). The resulting solution was warmed to room temperature and stirred overnight. The solvent was removed under vacuum and the residue extracted with dichloromethane (30 mL). The resulting solution was filtered through Celite and silica gel to remove LiBr. The filtrate was concentrated to a volume of 3 mL. Et₂O (20 mL) was then added, resulting in the formation of a white precipitate, which was removed by filtration. The filtrated solution was purified by chromatography over silica gel using hexane/ethyl acetate (1:1, v/v). Compound **2-Br** was dried in vacuum and obtained as a white solid. Further washing with *n*-pentane (20 mL) and drying afforded 0.62 g of **2-Br** (57 % yield). Single crystals of **2-Br** were obtained as colorless blocks by slow diffusion of hexanes into a CH₂Cl₂ solution of the compound. ¹H NMR (500 MHz, CDCl₃) δ 7.74 – 7.68 (m, 6H), 7.66 – 7.61 (m, 1H), 7.53 – 7.43 (m, 3H), 7.24 (d, *J* = 7.9 Hz, 6H), 7.13 (dt, *J* = 4.4, 2.6 Hz, 3H), 7.10 – 7.05 (m, 2H), 2.37 (s, 9H). ¹³C NMR (126 MHz, CDCl₃) δ 147.41 (s), 141.81(s), 137.36(s), 135.49(s), 135.23(s), 135.17(s), 134.37(s), 132.17(s), 130.41(s), 129.86(s), 129.72(s), 129.34(s), 129.16(s), 127.23(s), 21.50(s). ESI-MS calcd for C₃₃H₃₀SSb⁺ [M]⁺ 579.1101, found 579.1099.

Synthesis of [*o*-PhS(C₆H₄)SbPh₃][BF₄] ([1][BF₄]**):** AgBF₄ (200 mg, 1 mmol) was added to a CH₂Cl₂ solution of **1-Br** (300 mg, 0.49 mmol). The reaction mixture was stirred in the absence of light for 3 hours. The solution was filtered through Celite to remove AgBr and AgBF₄. The filtrate was evaporated to dryness and the residue recrystallized from Et₂O/CH₂Cl₂ to afford 240 mg of **[1][BF₄]** (80 % yield). Single crystals of **[1][BF₄]** were obtained as a colorless blocks by slow diffusion of hexanes into a CH₂Cl₂ solution of the salt. ¹H NMR (499 MHz, CDCl₃) δ 7.78 – 7.718 (m, 10H), 7.67 – 7.62 (m, 3H), 7.61 – 7.57 (m, 6H), 7.12 – 7.09 (m, 3H), 6.78 (dd, *J* = 6.3, 3.2 Hz, 2H). ¹³C NMR (100 MHz, CDCl₃) δ 139.22 (s), 137.62 (s), 137.01 (s), 135.49 (s), 135.24 (s), 134.00 (s), 133.63 (s), 132.86 (s), 131.87 (s), 131.28 (s), 129.52 (s), 127.68 (s), 127.47 (s), 122.74 (s). ¹⁹F NMR (470 MHz, CDCl₃) δ -151.39 (s), -151.45 (s). ESI-MS calcd for C₃₀H₂₄SSb⁺ [M]⁺ 537.0631, found 537.0620.

Synthesis of [*o*-PhS(C₆H₄)Sb(*p*-Tol)₃][BF₄] ([2][BF₄]**):** AgBF₄ (143 mg, 0.7 mmol) was added to a CH₂Cl₂ solution of **2-Br** (300 mg, 0.51 mmol). The reaction mixture was stirred in the absence of light for 3 hours. The solution was filtered through Celite to remove AgBr and AgBF₄. The filtrate was evaporated to dryness and the residue recrystallized from Et₂O/CH₂Cl₂ to afford 245 mg of **[2][BF₄]** (72 % yield). Single crystals of **[2][BF₄]** were obtained as a colorless blocks by slow diffusion of hexanes into a CDCl₃ solution of the salt. ¹H NMR (499 MHz, CDCl₃) δ 7.77 – 7.68 (m, 4H), 7.58 – 7.54 (m, 6H), 7.39 (d, *J* = 7.6 Hz, 6H), 7.10 (dd, *J* = 5.1, 2.0 Hz, 3H), 6.78 – 6.73 (m, 2H), 2.42 (s, 9H). ¹³C NMR (126 MHz, CDCl₃) δ 144.41(s), 139.06 (s), 137.65 (s), 136.93 (s), 135.20 (s), 135.09 (s), 134.30 (s), 131.84 (s), 131.72 (s), 129.38 (s), 127.71 (s), 127.17 (s), 119.33 (s), 21.70 (s). ¹⁹F NMR (470 MHz, CDCl₃) δ -152.38(s), -152.44(s). ESI-MS calcd for C₃₃H₃₀SSb⁺ [M]⁺ 579.1101, found 579.1098.

Synthesis of [*o*-MePhS(C₆H₄)SbPh₃][BF₄]₂ ([3][BF₄]₂**):** In a 25 mL Schlenk tube, [Me₃O][BF₄] (100 mg, 0.7 mmol) was added to **[1][BF₄]** (150 mg, 0.24 mmol) dissolved in a mixture of toluene (5 mL) and CH₂Cl₂ (2 mL). The Schlenk tube was sealed under N₂ and the resulting mixture was stirred at 90 °C overnight behind a glass shield. The solvents were evaporated to dryness and the residue was extracted with dichloromethane (20 mL). The resulting solution was filtered over Celite to remove [Me₃O][BF₄]. The filtrate was concentrated to a volume of 3 mL. Et₂O (20 mL) was then added, resulting in the formation of a white precipitate, which was collected by filtration

and washed with Et₂O and *n*-pentane to afford [3][BF₄]₂ (0.13 g, 75 % yield). ¹H NMR (499 MHz, CD₂Cl₂) δ 8.21 (dd, *J* = 8.2, 1.2 Hz, 1H), 8.06 (td, *J* = 7.9, 1.4 Hz, 1H), 7.93 (td, *J* = 7.6, 1.2 Hz, 1H), 7.81 – 7.73 (m, 10H), 7.72 – 7.63 (m, 7H), 7.55 – 7.48 (m, 2H), 7.24 (d, *J* = 7.6 Hz, 2H), 3.43 (s, 3H). ¹³C NMR (126 MHz, CD₂Cl₂) δ 138.07 (s), 136.04 (s), 135.96 (s), 135.74 (s), 134.62 (s), 134.01 (s), 133.45 (s), 131.53 (s), 131.46 (s), 131.17 (s), 129.06 (s), 124.85 (s), 124.22 (s), 30.00 (s). ¹⁹F NMR (470 MHz, CD₂Cl₂) δ -148.96 (s), -149.01(s). ESI-MS calcd for C₃₁H₂₇SSb²⁺ [M]²⁺ 276.0424, found 276.0430.

Isolation of [3]₂[μ₂-F][BF₄]₃: Single crystals of [3]₂[μ₂-F][BF₄]₃ were obtained as colorless blocks by diffusion of pentanes into a CH₂Cl₂ solution of [3][BF₄]₂. The single crystals were filtered and washed with hexanes prior to NMR analysis. ¹H NMR (499 MHz, CD₂Cl₂) δ 8.13 (dd, *J* = 8.2, 1.2 Hz, 1H), 7.93 (td, *J* = 7.9, 1.5 Hz, 1H), 7.80 (td, *J* = 7.6, 1.1 Hz, 1H), 7.76 – 7.69 (m, 3H), 7.68 – 7.55 (m, 14H), 7.47 – 7.40 (m, 2H), 7.09 (d, *J* = 8.0 Hz, 2H), 3.15 (s, 3H). ¹³C NMR (126 MHz, CD₂Cl₂) δ 138.62 (s), 137.68 (s), 135.66 (s), 135.55 (s), 135.37 (s), 135.11 (s), 134.43 (s), 133.64 (s), 131.38 (s), 131.30 (s), 128.99 (s), 126.81 (s), 124.27 (s), 29.25 (s). ¹⁹F NMR (470 MHz, CD₂Cl₂) δ -57.00 (s), -149.43 (s), -149.49 (s).

Synthesis of [o-MePhS(C₆H₄)Sb(*p*-Tol)₃][BF₄]₂ ([4][BF₄]₂): In a 25 mL Schlenk tube, [Me₃O][BF₄] (100 mg, 0.7 mmol) was added to [2][BF₄] (160 mg, 0.24 mmol) dissolved in toluene (5 mL). The Schlenk tube was sealed under N₂ and the resulting mixture was stirred at 90 °C overnight behind a glass shield. The solvents were evaporated to dryness and the residue was extracted with dichloromethane (20 mL). The resulting solution was filtered over Celite to remove [Me₃O][BF₄]. The filtrate was concentrated to a volume of 3 mL. Et₂O (20 mL) was then added, resulting in the formation of a white precipitate, which was collected by filtration and washed with Et₂O and *n*-pentane to afford [4][BF₄]₂ (0.18 g, 58 % yield). ¹H NMR (499 MHz, CD₂Cl₂) δ 8.27 (dd, *J* = 8.2, 1.2 Hz, 1H), 8.12 (t, *J* = 7.5 Hz, 1H), 7.99 (t, *J* = 7.7 Hz, 1H), 7.83 – 7.79 (m, 1H), 7.72 – 7.64 (m, 7H), 7.54 (dd, *J* = 8.1, 2.8 Hz, 8H), 7.31 (d, *J* = 7.7 Hz, 2H), 3.51 (s, 3H), 2.51 (s, 9H). ¹³C NMR (126 MHz, CD₂Cl₂) δ 145.97 (s), 138.40 (s), 136.69 (s), 136.40 (s), 135.48 (s), 134.54 (s), 133.78 (s), 132.47 (s), 131.76 (s), 131.46 (s), 130.76 (s), 129.07 (s), 124.17 (s), 118.27 (s), 30.16 (s), 21.51 (s). ¹⁹F NMR (470 MHz, CD₂Cl₂) δ -149.25(s), -149.31(s). ESI-MS calcd for C₃₄H₃₃SSb²⁺ [M]²⁺ 297.0665, found 297.0666.

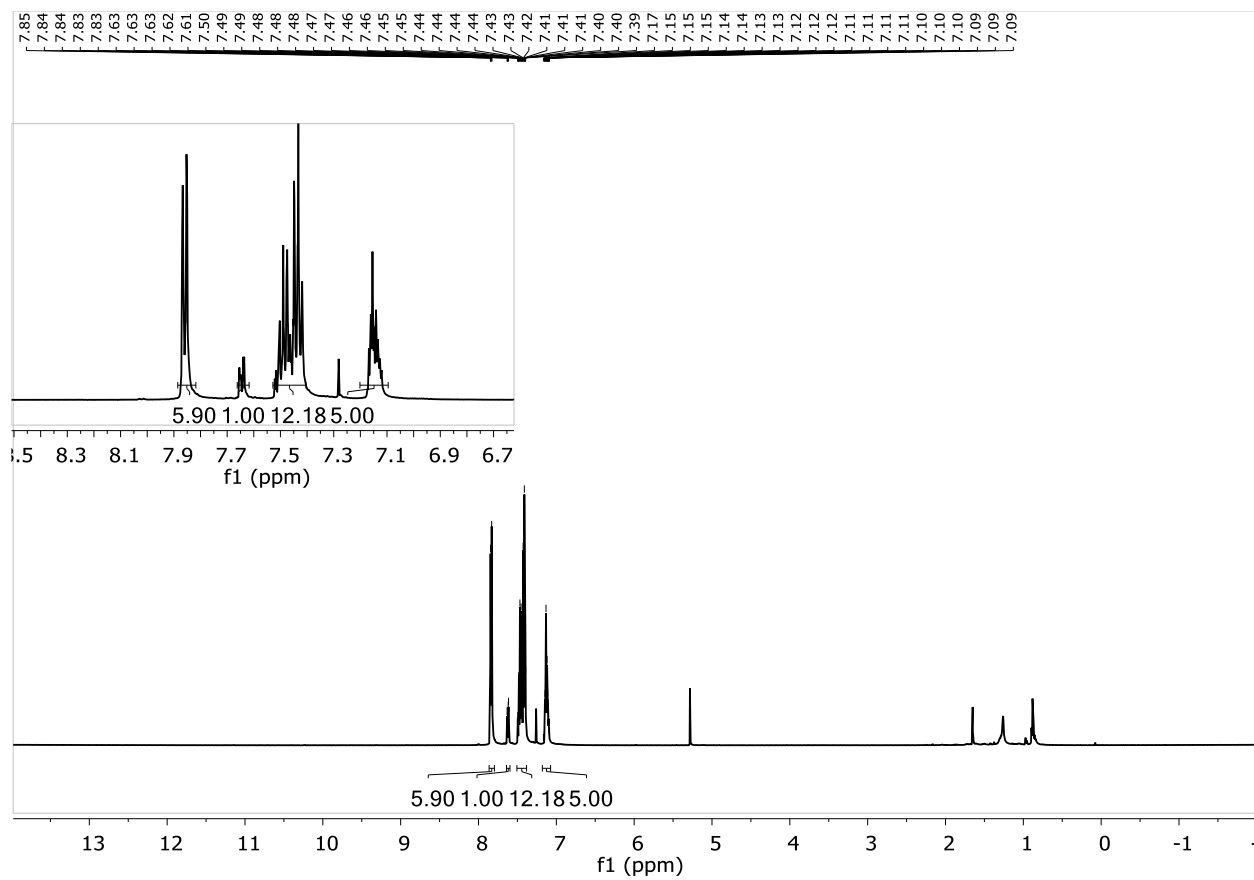


Figure S1. ^1H NMR spectrum of 1-Br in CDCl_3 .

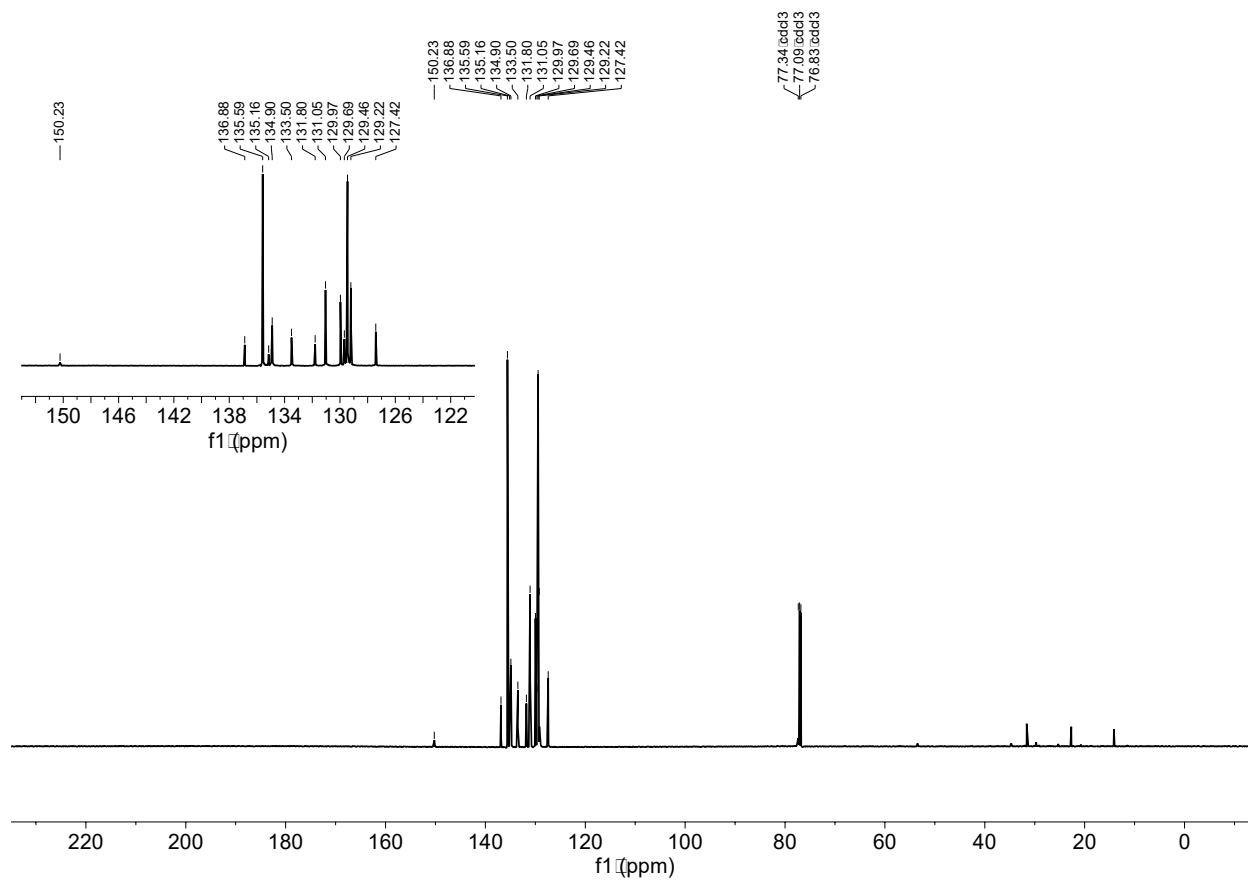


Figure S2. ^{13}C NMR spectrum of 1-Br in CDCl_3 .

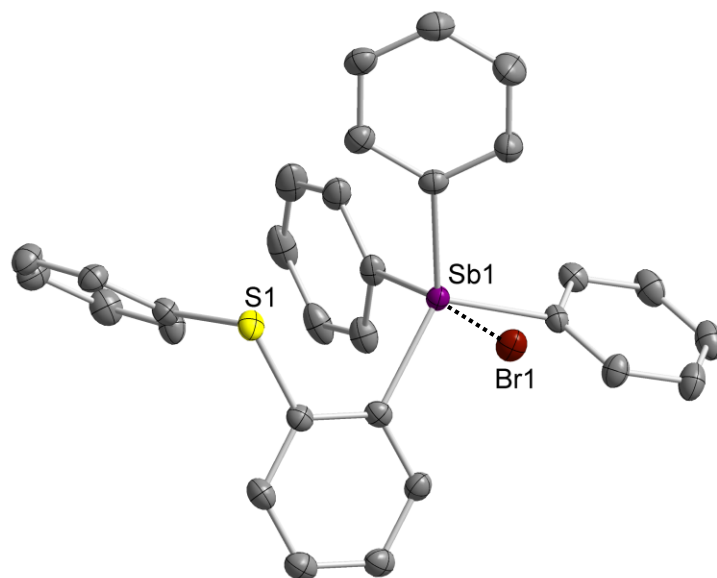


Figure S3. Structure of **1-Br** in the crystal. Ellipsoids are drawn at the 50% probability level. The hydrogen atoms are omitted for clarity.

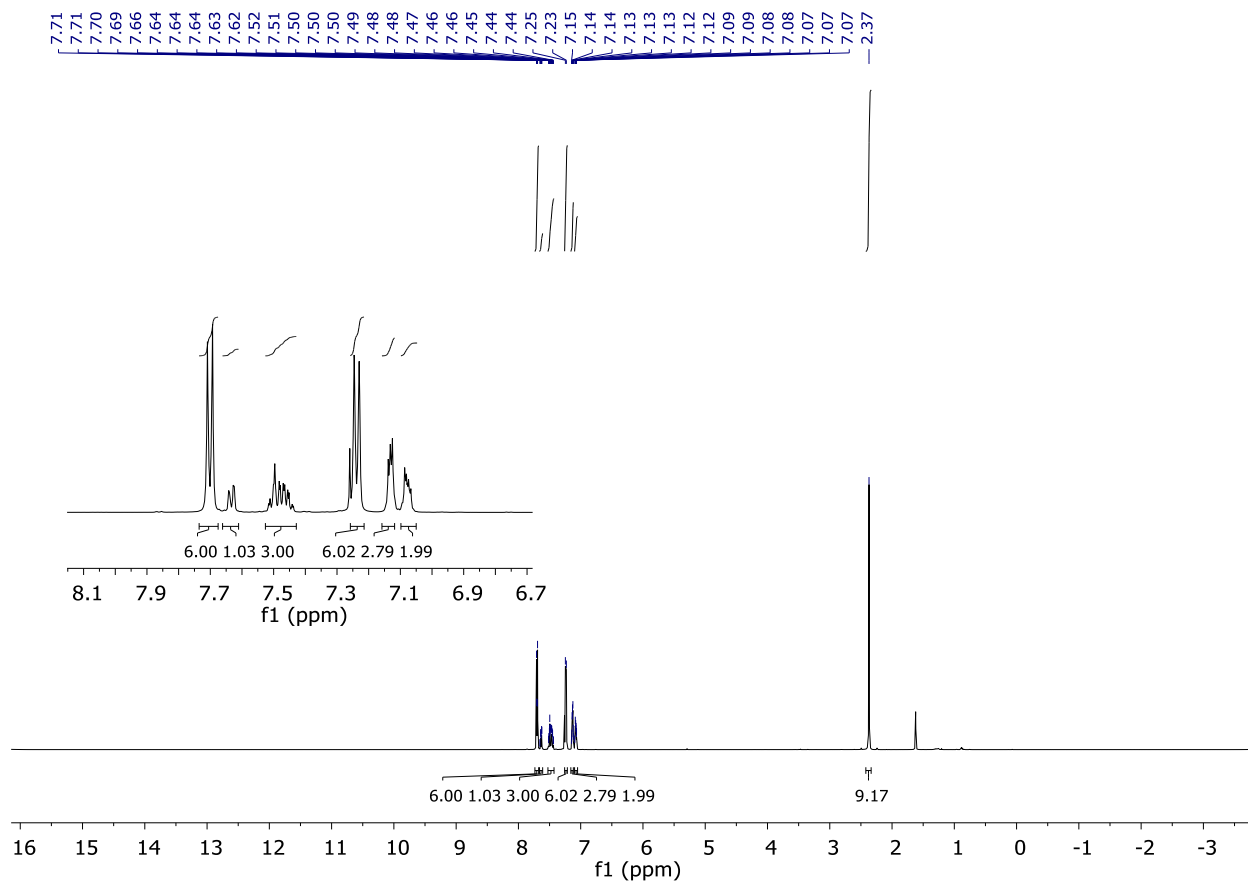


Figure S4. ^1H NMR spectrum of **2-Br** in CDCl_3 .

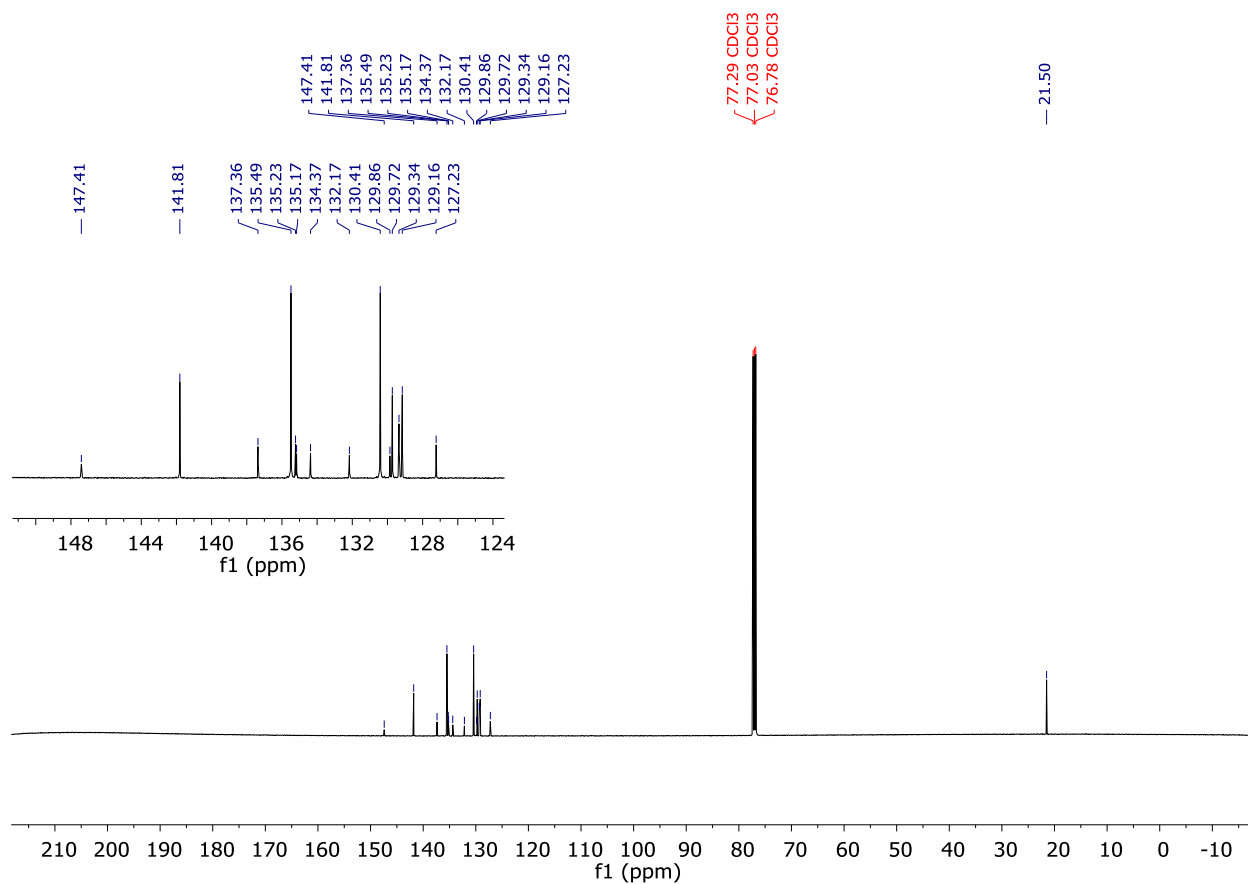


Figure S5. ^{13}C NMR spectrum of 2-Br in CDCl_3 .

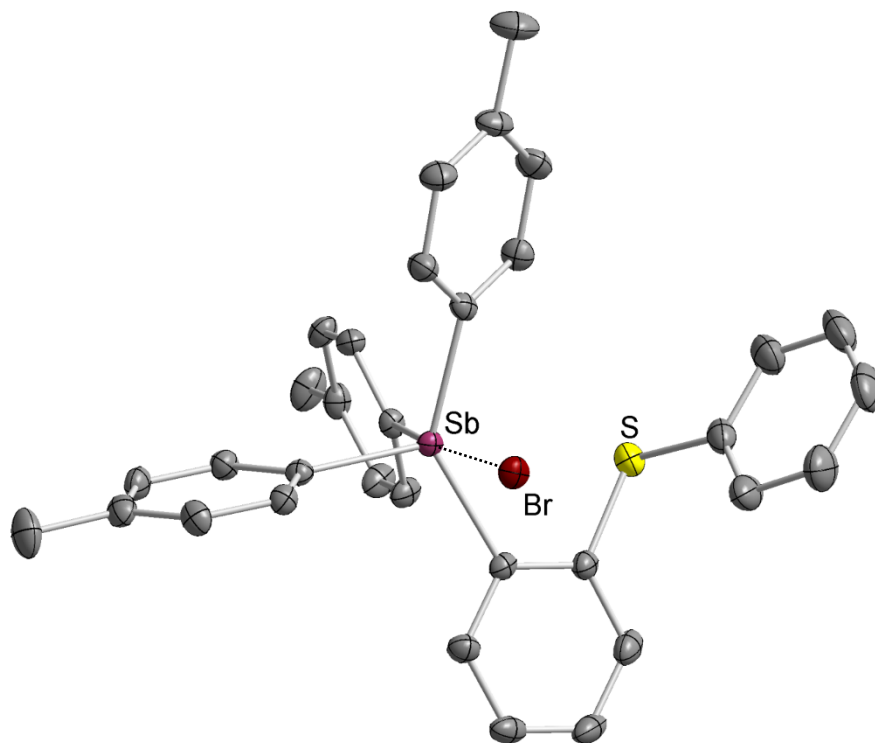


Figure S6. Structure of 2-Br in the crystal. Ellipsoids are drawn at the 50% probability level. The hydrogen atoms are omitted for clarity.

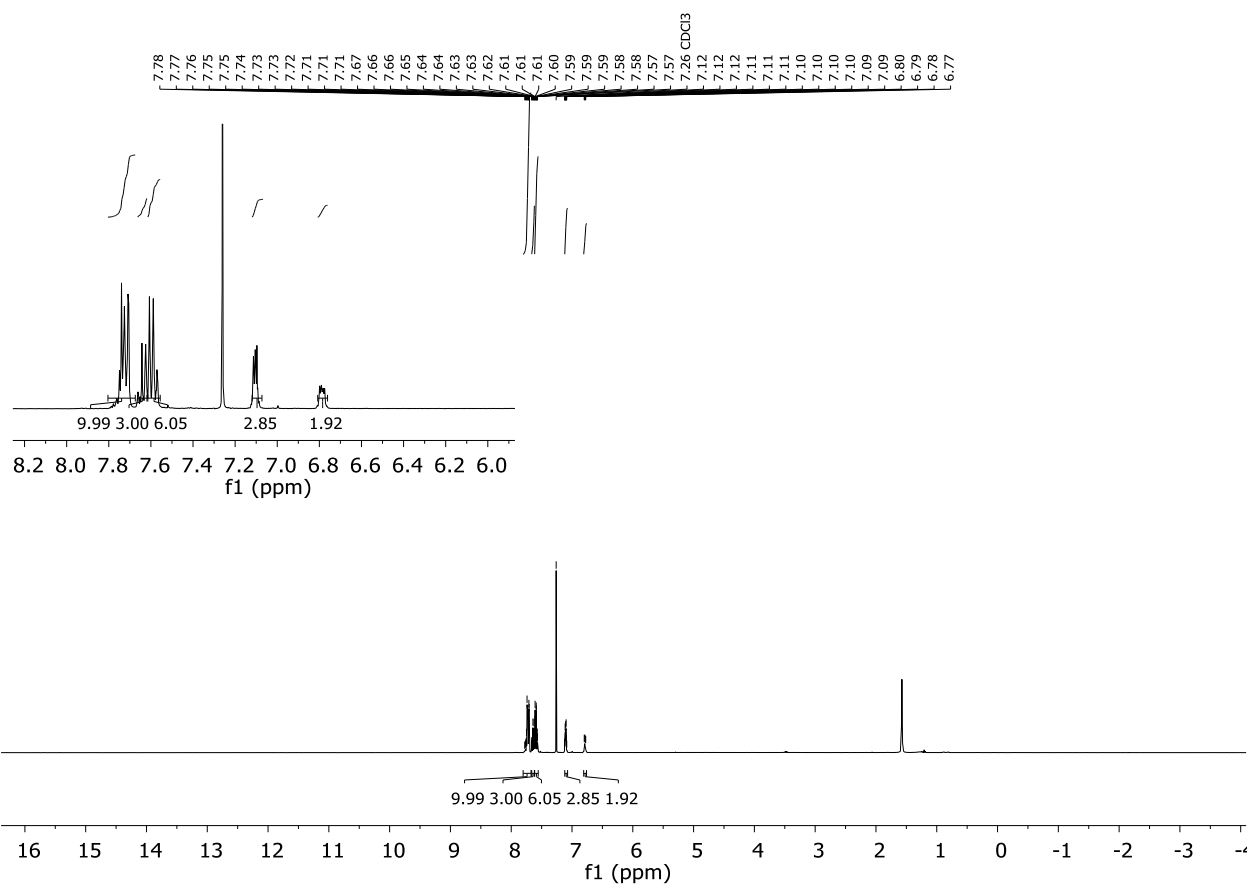


Figure S7. ^1H NMR spectrum of $[\mathbf{1}][\text{BF}_4]$ in CDCl_3 .

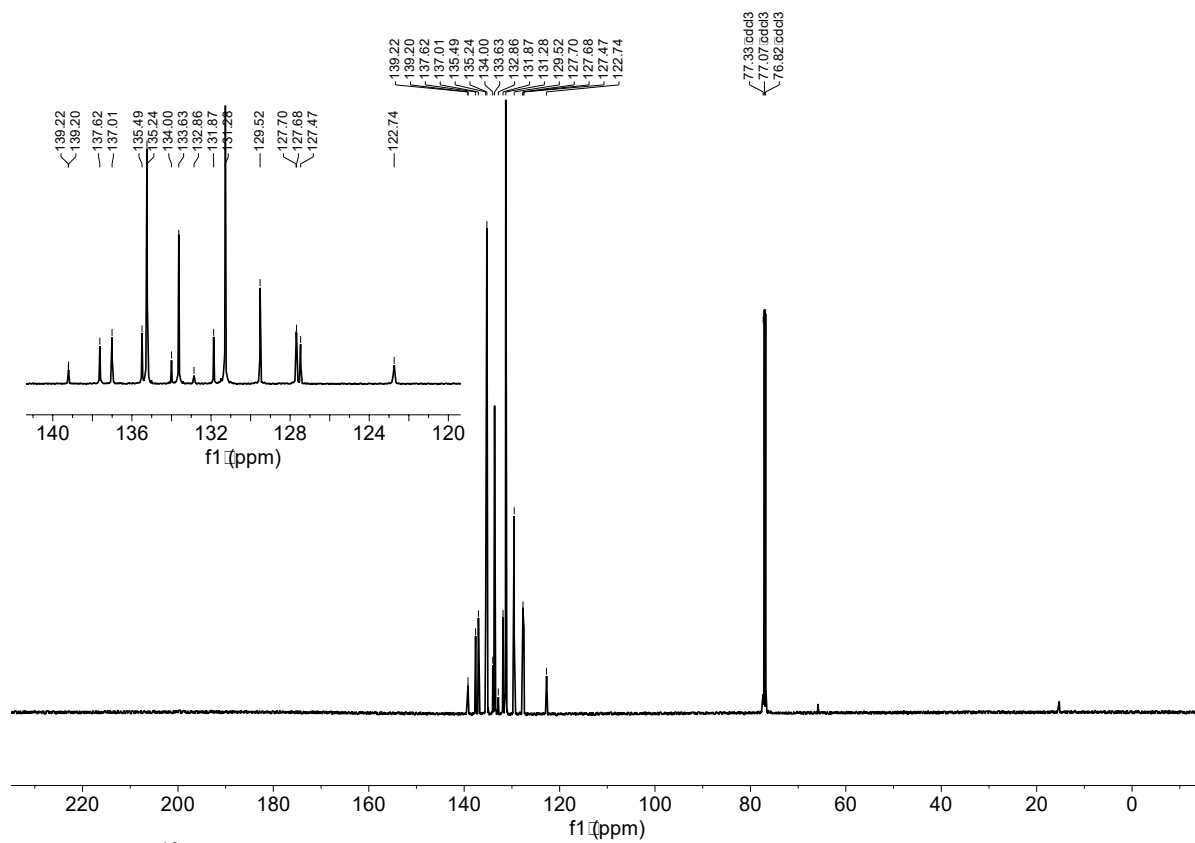


Figure S8. ^{13}C NMR spectrum of $[\mathbf{1}][\text{BF}_4]$ in CDCl_3 .

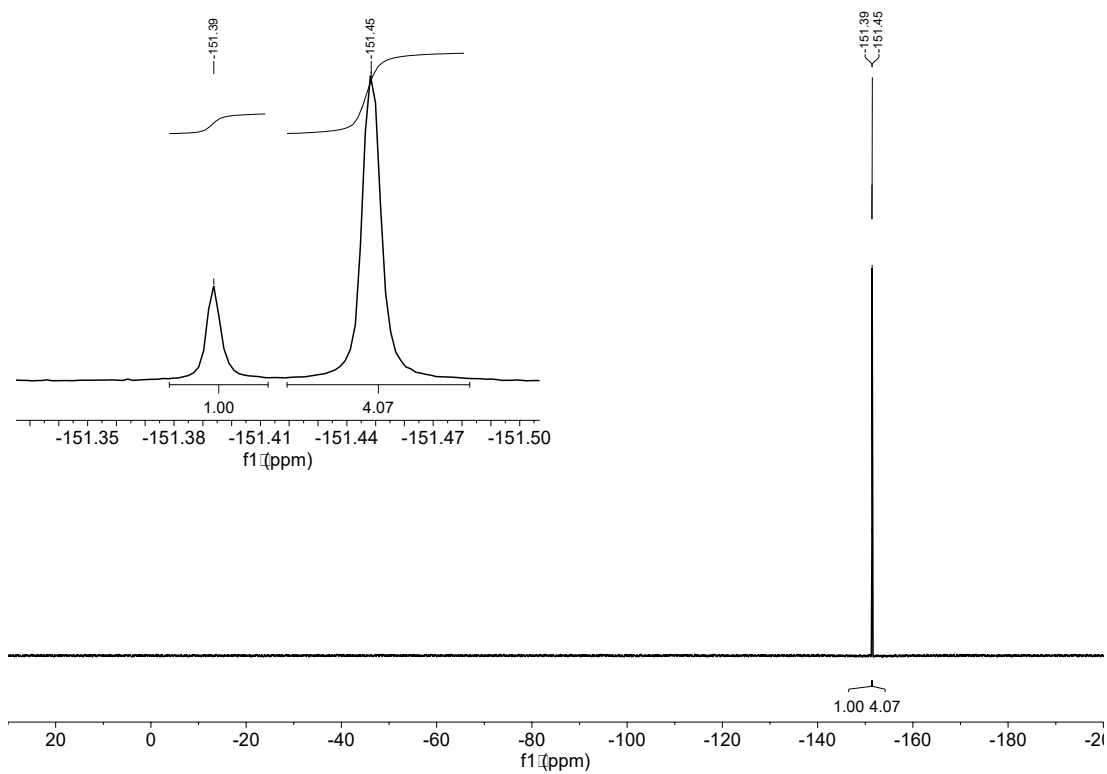


Figure S9. ^9F NMR spectrum of $[\mathbf{1}][\text{BF}_4]$ in CDCl_3 .

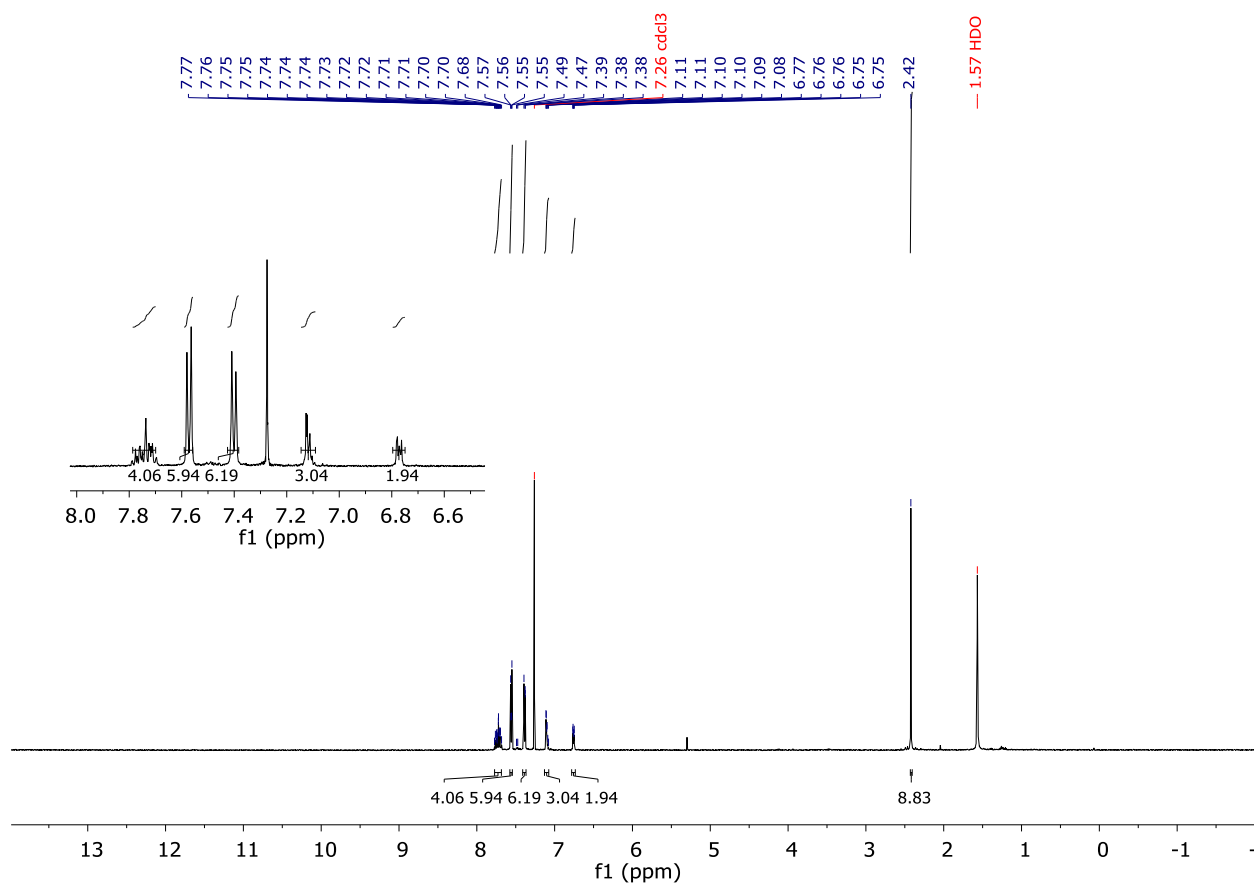


Figure S10. ^1H NMR spectrum of $[\mathbf{2}][\text{BF}_4]$ in CDCl_3 .

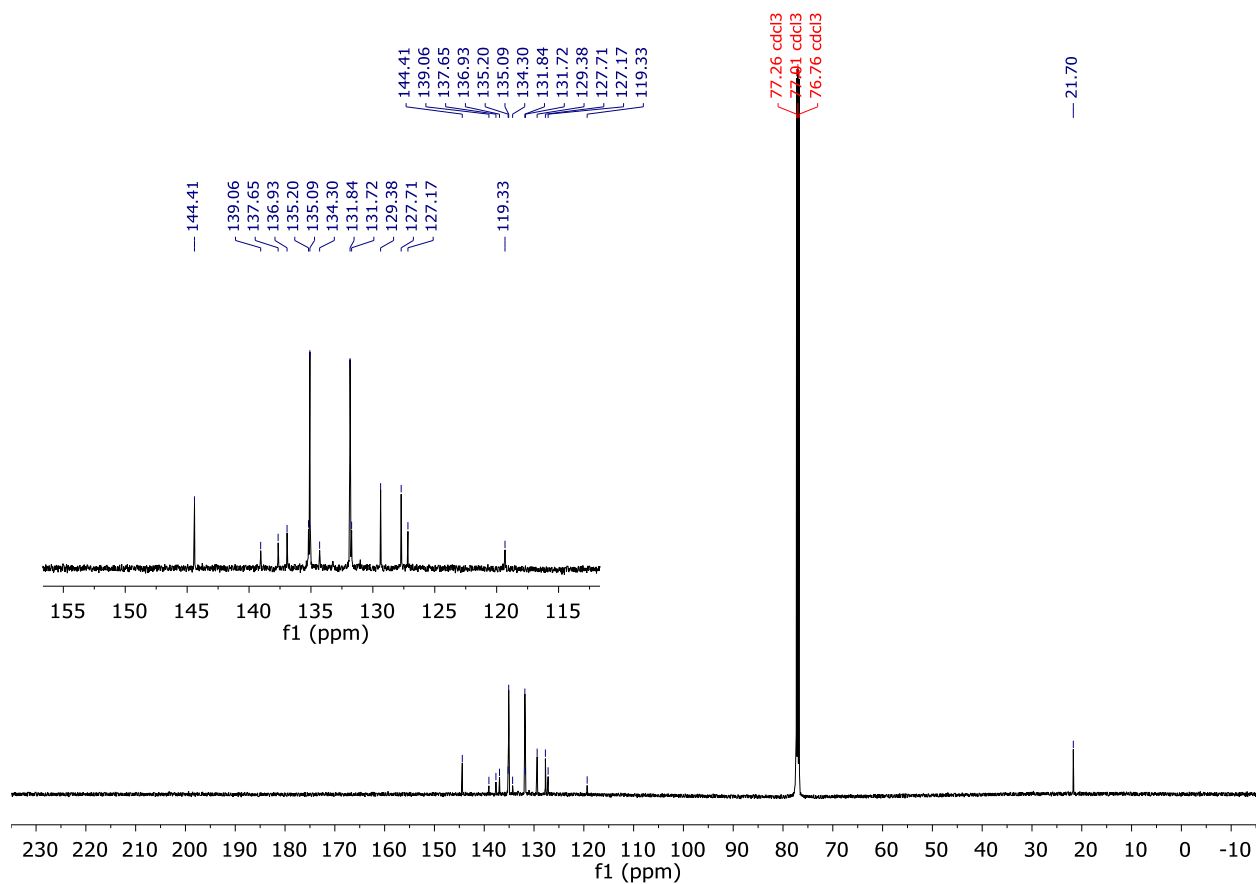


Figure S11. ^{13}C NMR spectrum of $[\mathbf{2}][\text{BF}_4]$ in CDCl_3 .

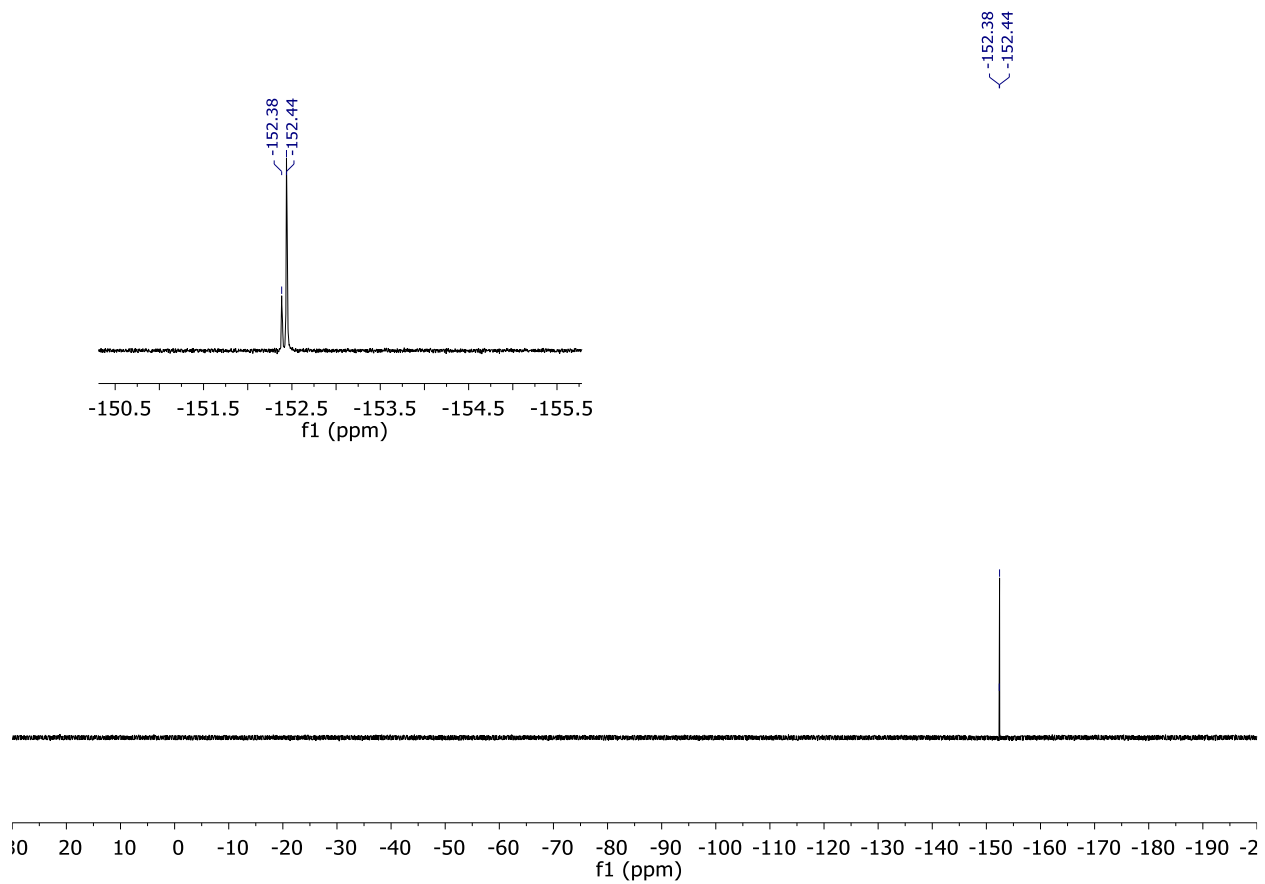


Figure S12. ${}^9\text{F}$ NMR spectrum of $[\mathbf{2}][\text{BF}_4]$ in CDCl_3 .

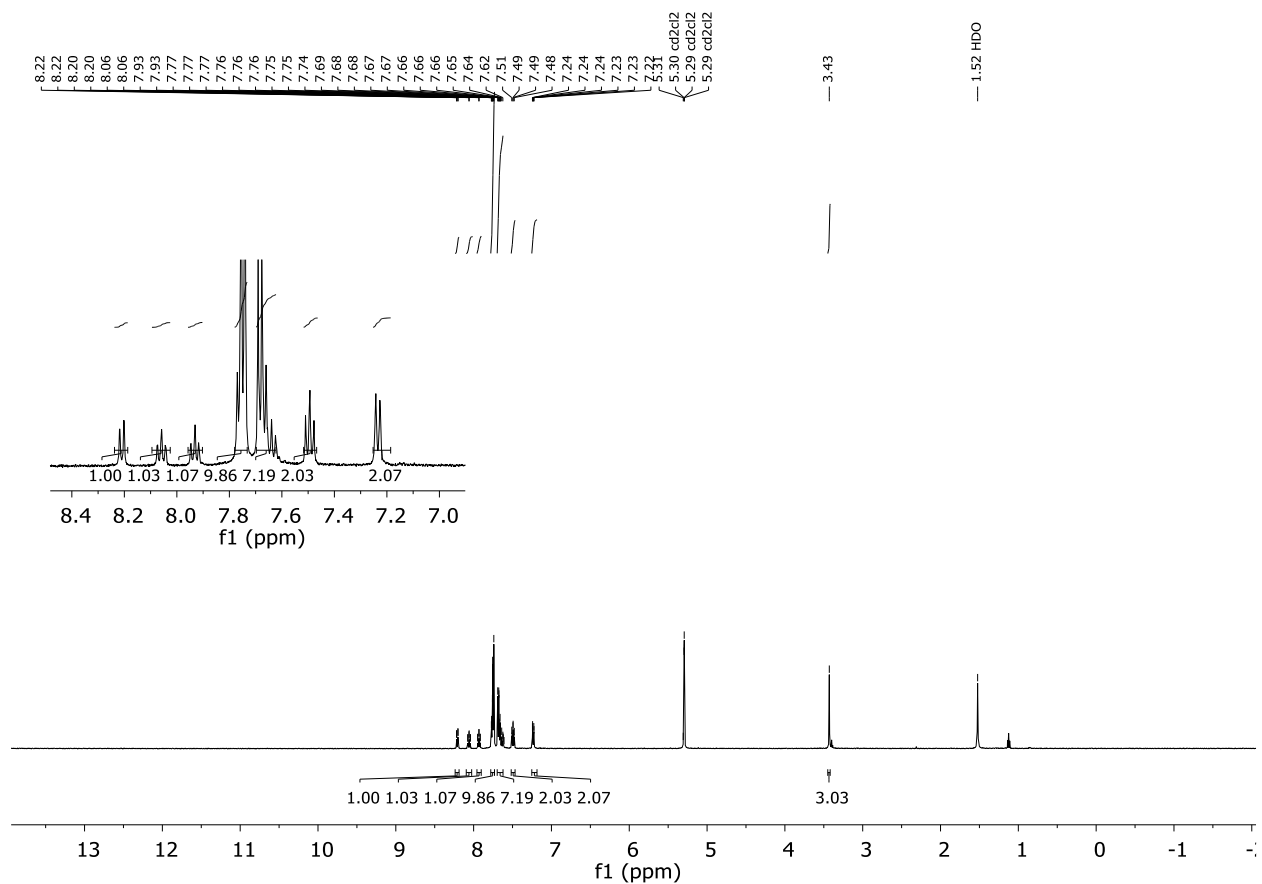


Figure S13. ¹H NMR spectrum of [3][BF₄]₂ in CD₂Cl₂.

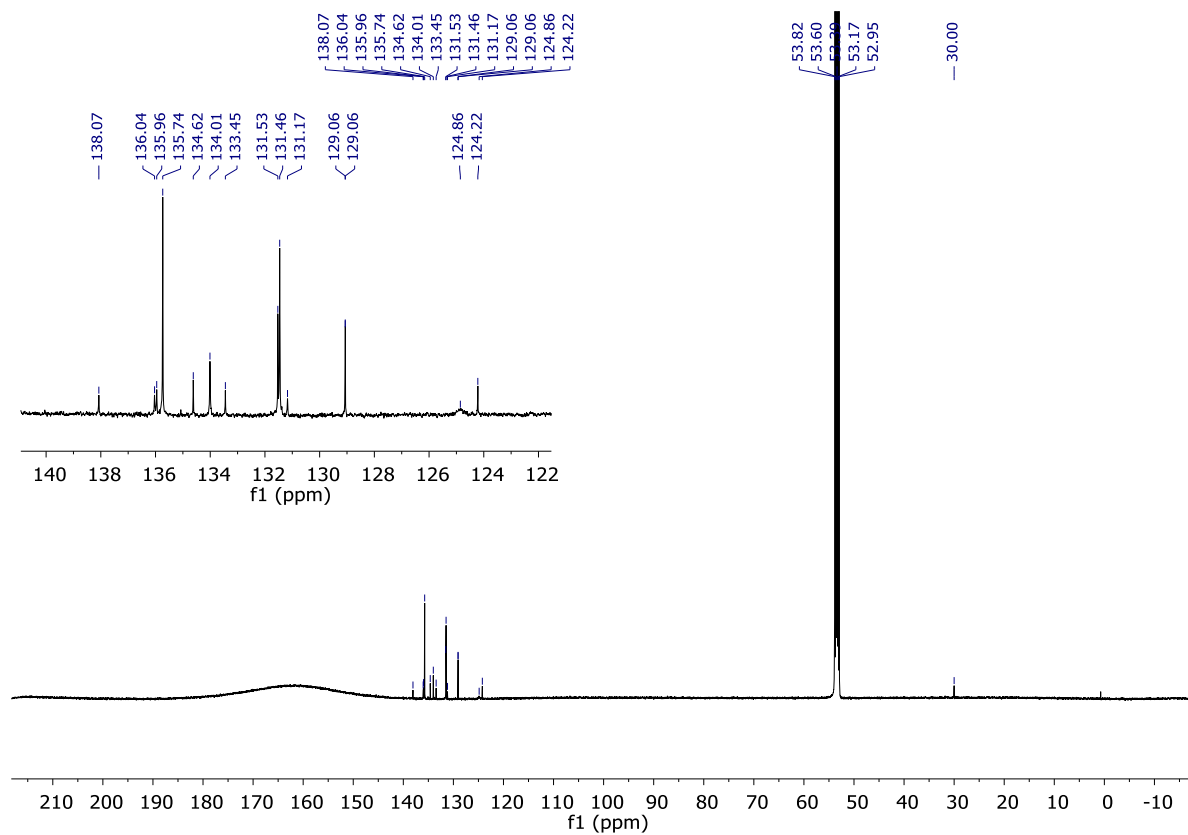


Figure S14. ^{13}C NMR spectrum of $[\mathbf{3}][\text{BF}_4]_2$ in CD_2Cl_2 .

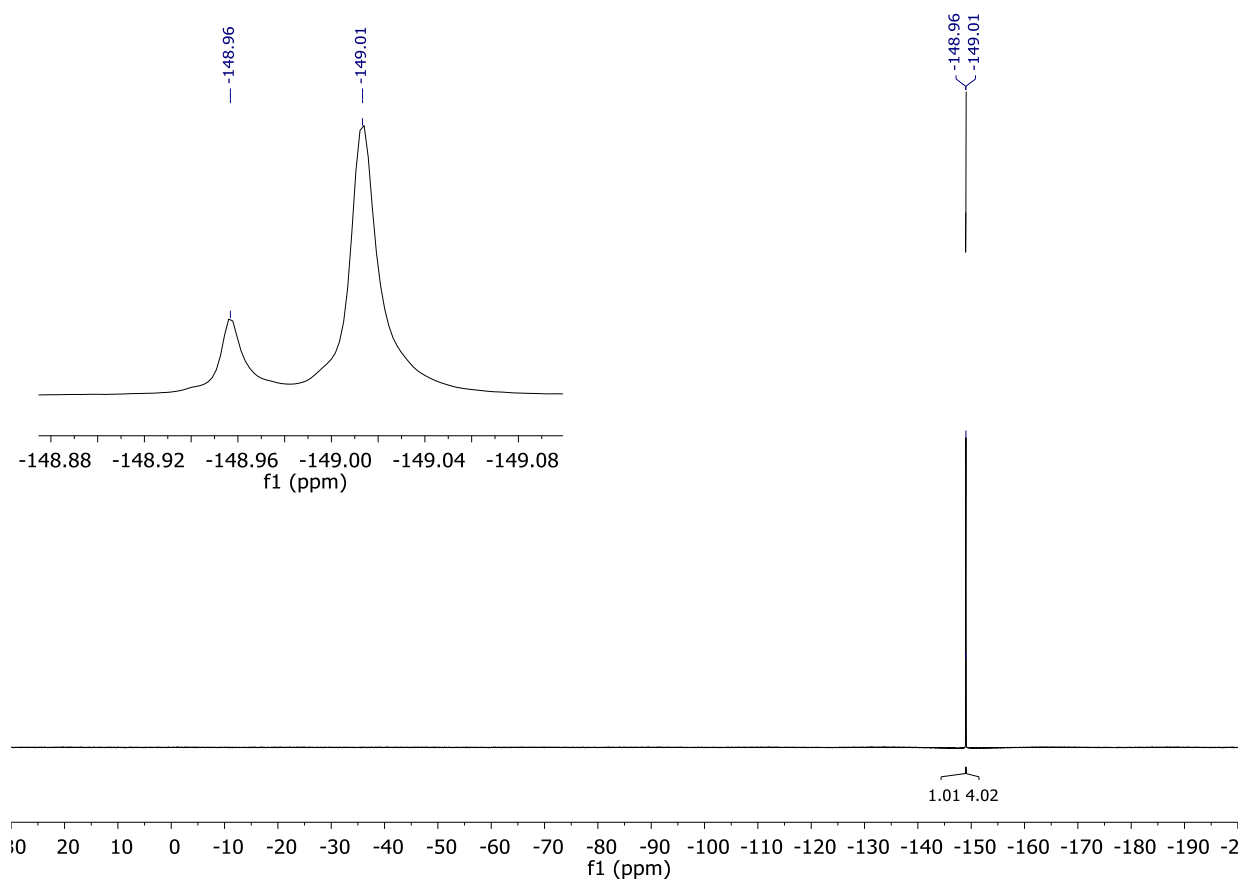


Figure S15. ${}^9\text{F}$ NMR spectrum of $[\mathbf{3}][\text{BF}_4]_2$ in CD_2Cl_2 .

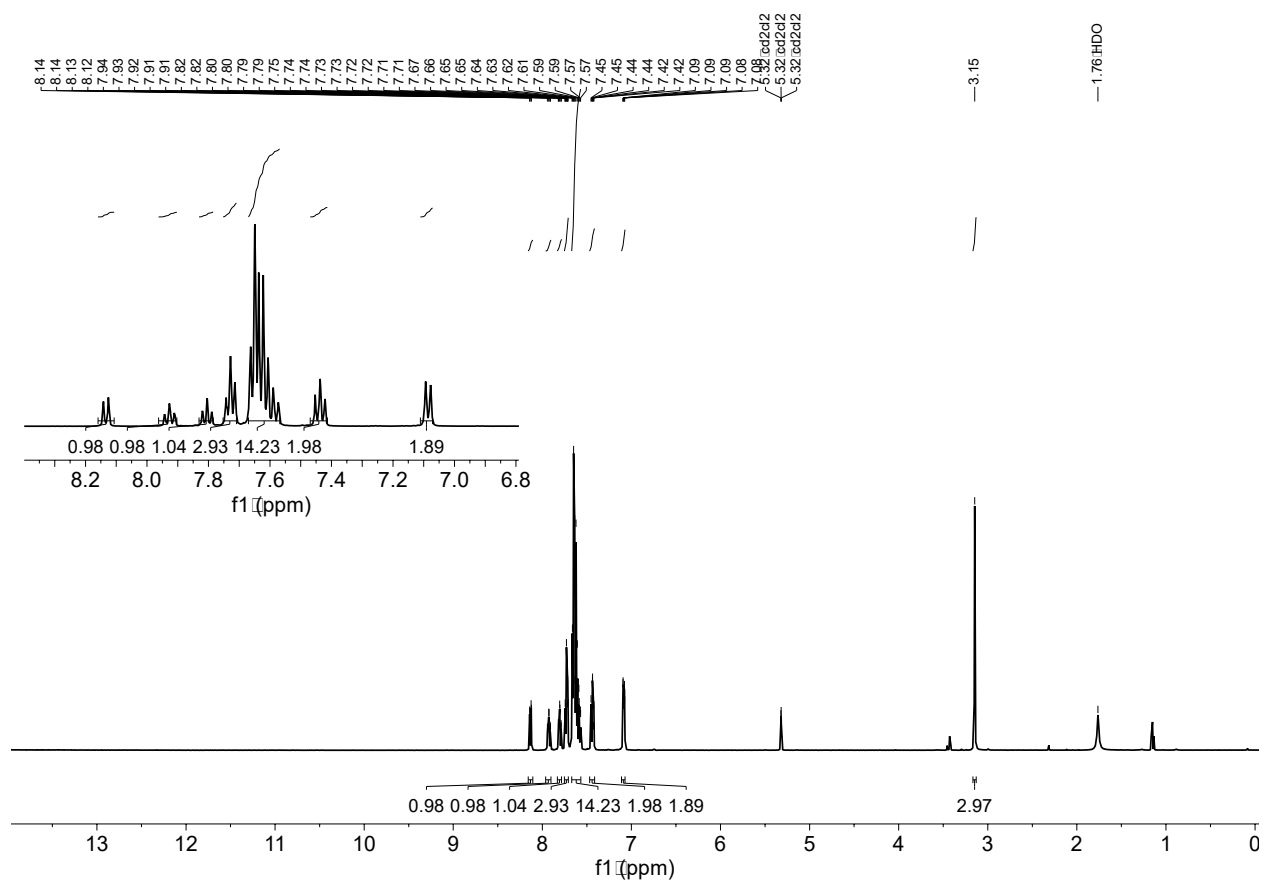


Figure S16. ^1H NMR spectrum of $[\mathbf{3}]_2[\mu_2\text{-F}][\text{BF}_4]_3$ in CD_2Cl_2 .

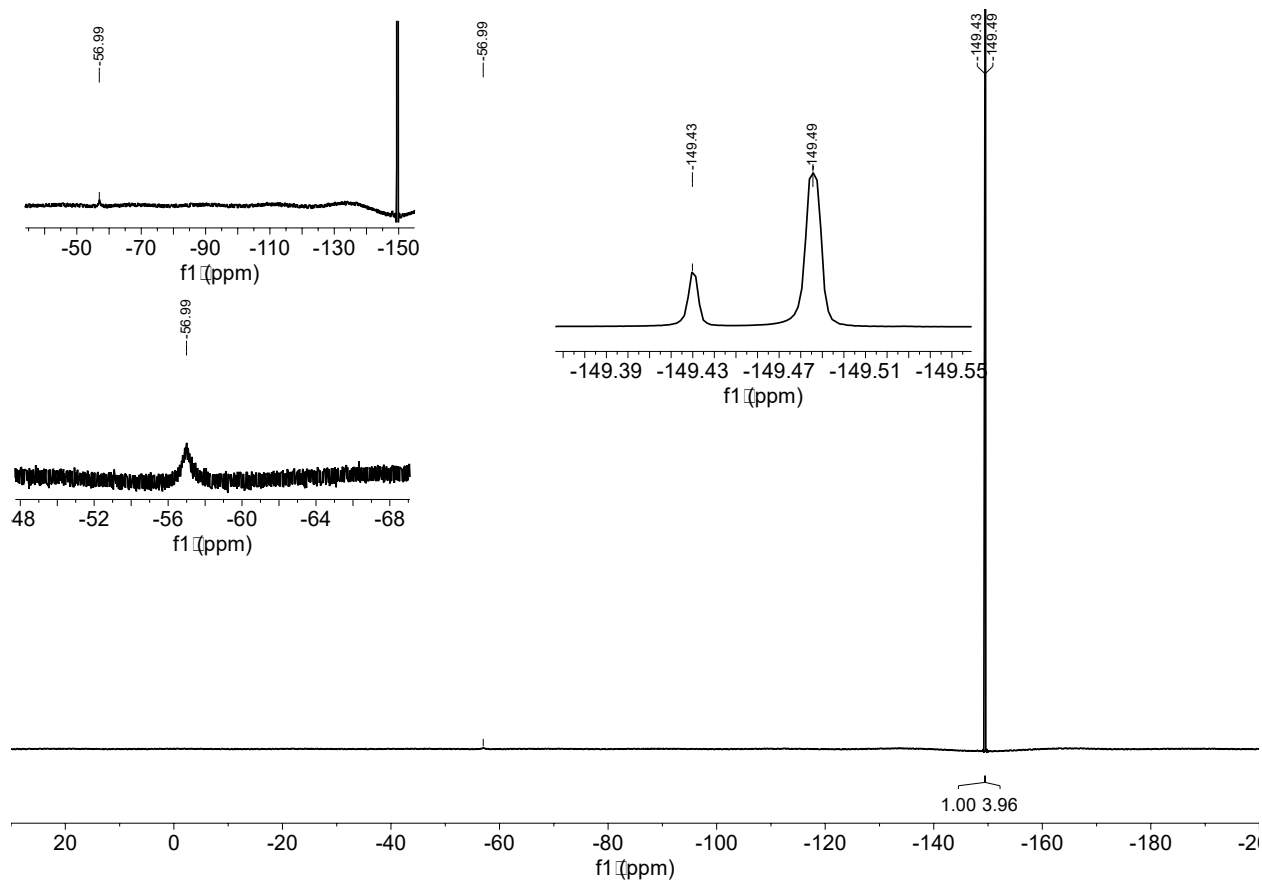


Figure S18. ^9F NMR spectrum of $[\mathbf{3}]_2[\mu_2\text{-F}][\text{BF}_4]_3$ in CD_2Cl_2 .

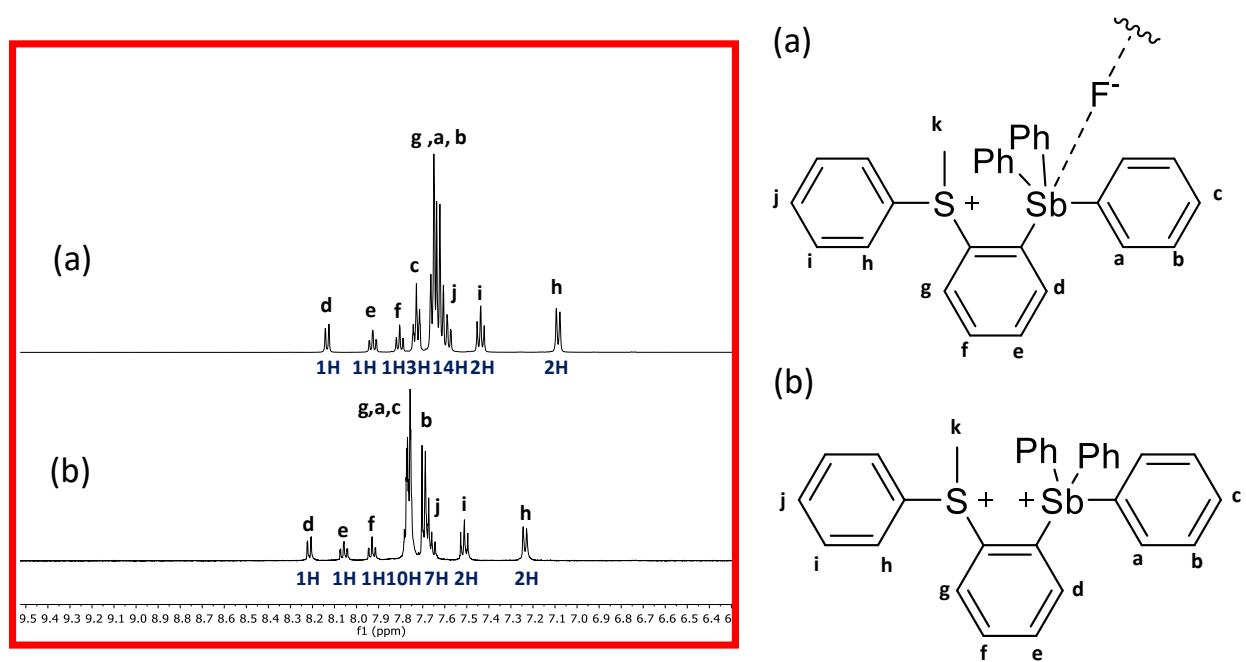
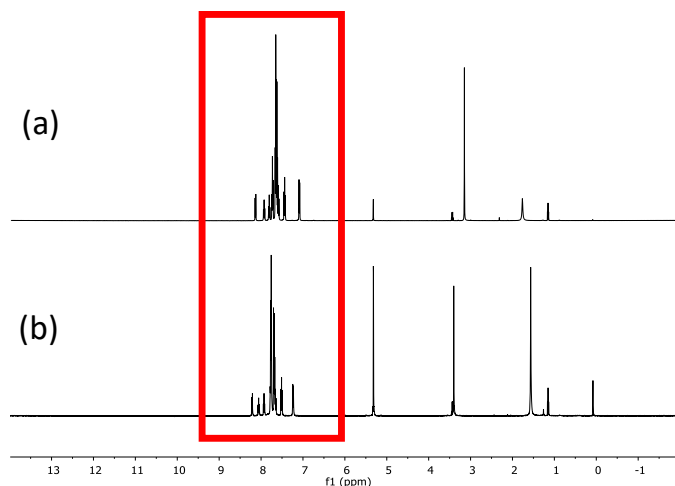


Figure S19. Top: ^1H NMR spectrum of (a) $[\mathbf{3}]_2[\mu_2\text{-F}][\text{BF}_4]_3$ and (b) $[\mathbf{3}][\text{BF}_4]_2$ in CD_2Cl_2 . Bottom: ^1H NMR spectrum in the aromatic region of (a) $[\mathbf{3}]_2[\mu_2\text{-F}][\text{BF}_4]_3$ and (b) $[\mathbf{3}][\text{BF}_4]_2$ in CD_2Cl_2 .

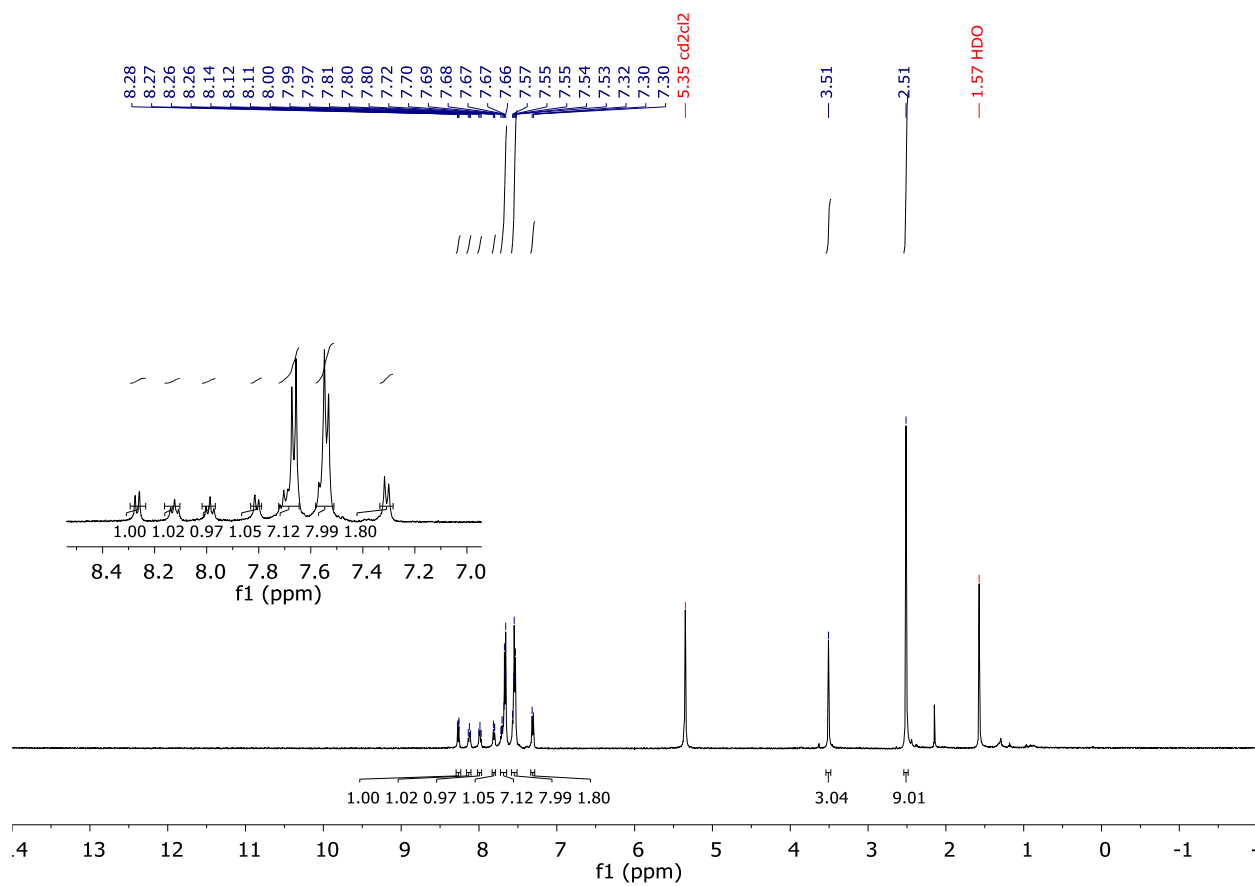


Figure S20. ^1H NMR spectrum of $[\mathbf{4}][\text{BF}_4]_2$ in CD_2Cl_2 .

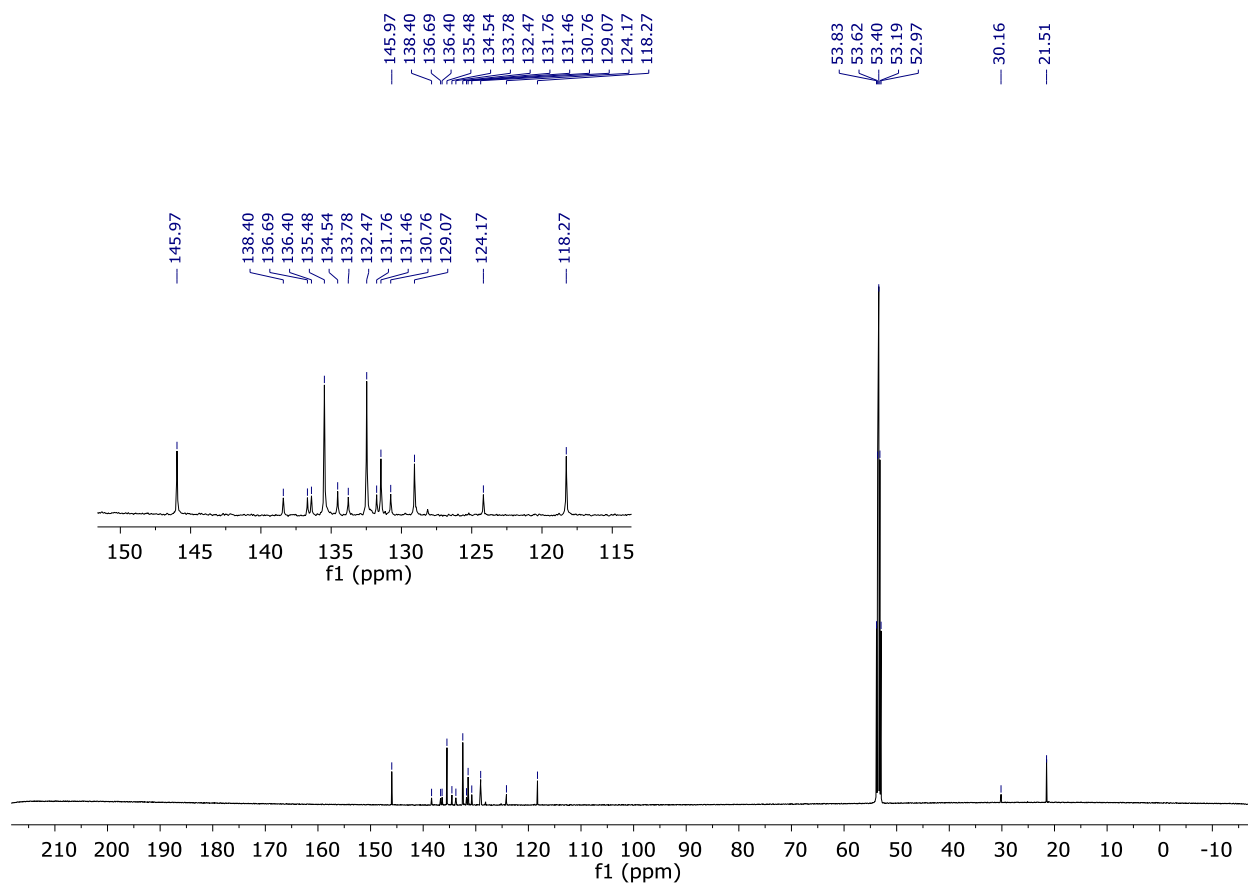


Figure S21. ^{13}C NMR spectrum of $[\mathbf{4}][\text{BF}_4]_2$ in CD_2Cl_2 .

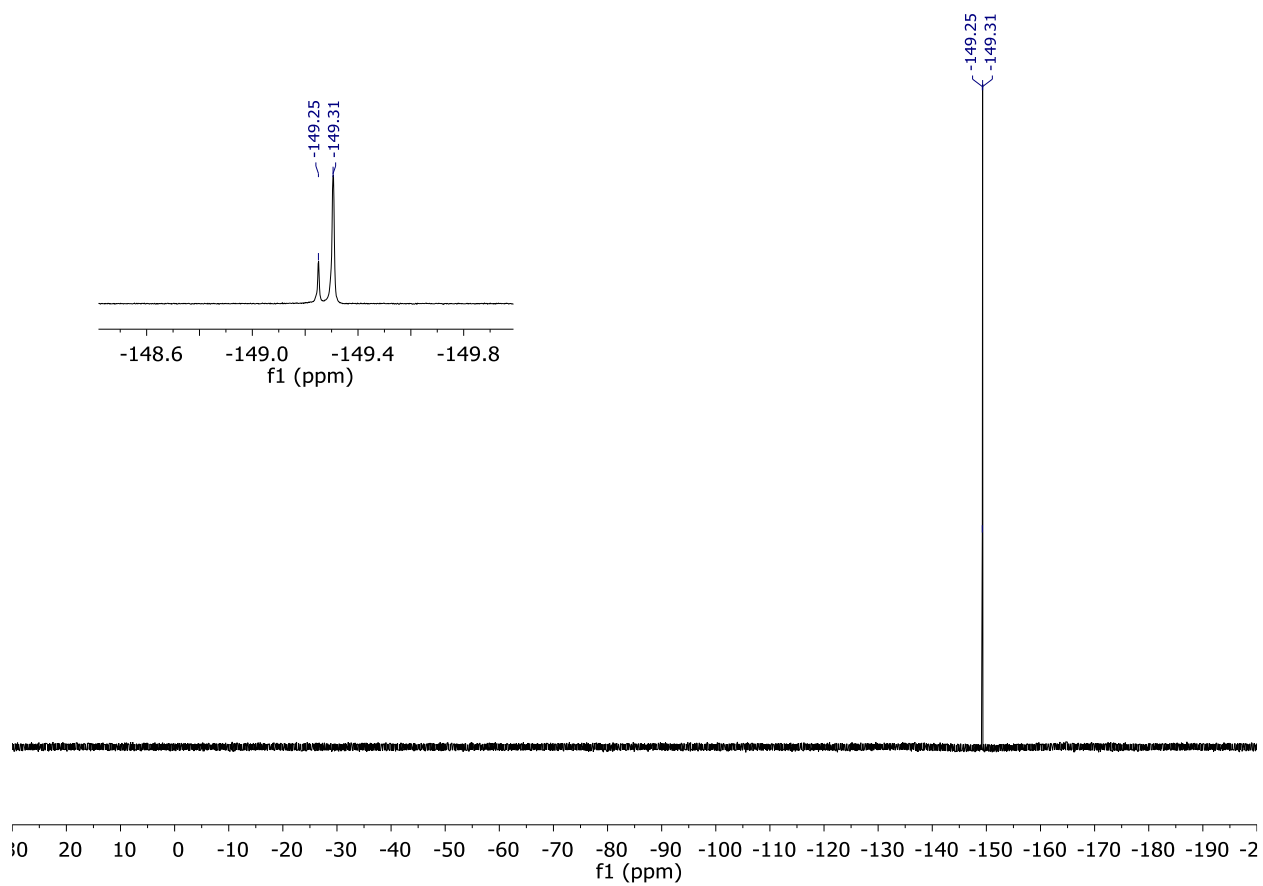
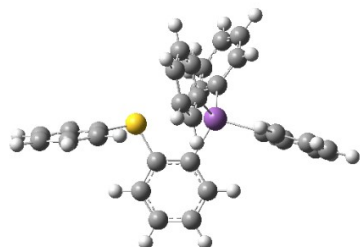


Figure S22. ^9F NMR spectrum of $[\mathbf{4}][\text{BF}_4]_2$ in CD_2Cl_2 .

Computational details

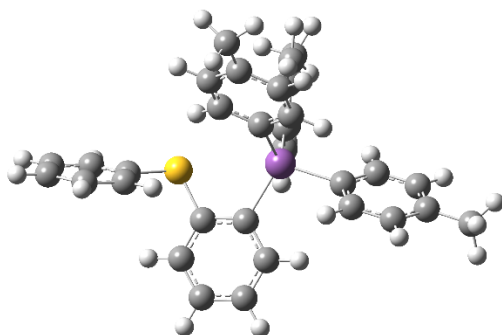
All calculations were carried out using density functional theory as implemented in the Gaussian 09 program⁵ All calculations were conducted with the B3LYP⁶ functional and mixed basis sets (cc-pVTZ⁷ with ECP28 MDF⁸ for Sb, 6-31+g(d) for the sulfur, cc-pVTZ for Cl, 6-31g for all carbon and hydrogen atoms) starting from the crystal structure geometries when available. No imaginary frequencies were found for the optimized structures, confirming that a local minimum on the potential energy hypersurface had in all cases been reached.

Table S1. XYZ coordinates of the optimized geometry of [1]⁺.



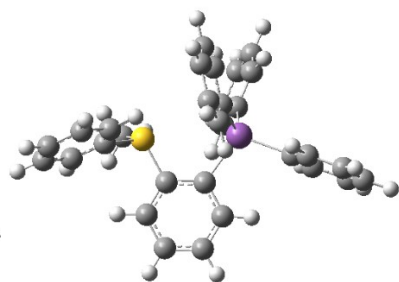
Sb	-1.029977	-0.005657	-0.013789	H	7.440185	-0.902380	-0.363020
S	2.165944	1.141024	0.168334	C	6.222508	0.832941	0.033240
C	-1.466742	1.925742	-0.761834	H	7.067521	1.503813	0.144197
C	-0.850960	3.068570	-0.222847	C	4.920808	1.327129	0.181720
H	-0.116219	2.988089	0.570506	H	4.754243	2.374987	0.406178
C	-1.191120	4.332519	-0.719105	C	-2.900670	-0.826143	0.561473
H	-0.718519	5.215885	-0.304028	C	-3.802339	-0.031077	1.295229
C	-2.135236	4.456041	-1.745394	H	-3.557189	0.993350	1.558738
H	-2.393202	5.437794	-2.127247	C	-5.038779	-0.561270	1.679503
C	-2.751464	3.316545	-2.277780	H	-5.734792	0.050797	2.242760
H	-3.487327	3.413360	-3.068569	C	-5.378128	-1.875343	1.332741
C	-2.424697	2.047751	-1.786856	H	-6.338727	-2.281718	1.630119
H	-2.923679	1.174500	-2.196099	C	-4.483892	-2.663680	0.598685
C	0.178526	0.003675	1.732585	H	-4.750701	-3.678702	0.325036
C	1.528984	0.418283	1.683238	C	-3.243390	-2.144182	0.210192
C	2.311858	0.316225	2.844799	H	-2.563751	-2.761295	-0.368040
H	3.349045	0.629885	2.816963	C	-0.226636	-1.269661	-1.508977
C	1.760170	-0.182023	4.028317	C	0.209210	-2.561018	-1.158158
H	2.379677	-0.256675	4.915512	H	0.162281	-2.908907	-0.130430
C	0.414705	-0.568627	4.079912	C	0.720183	-3.407869	-2.149111
H	-0.011933	-0.946730	5.002037	H	1.055543	-4.404749	-1.883844
C	-0.378870	-0.474000	2.933424	C	0.797053	-2.969343	-3.477170
H	-1.416425	-0.788352	2.972558	H	1.193572	-3.628560	-4.241637
C	3.826478	0.459575	0.035997	C	0.366771	-1.682008	-3.820478
C	4.033027	-0.897067	-0.264794	H	0.432755	-1.341742	-4.848101
H	3.185080	-1.559641	-0.398109	C	-0.146119	-0.825614	-2.839173
C	5.336520	-1.384022	-0.398639	H	-0.464154	0.174633	-3.114016
H	5.498375	-2.432293	-0.626530				
C	6.430921	-0.520923	-0.251580				

Table S2. XYZ coordinates of the optimized geometry of [2]⁺

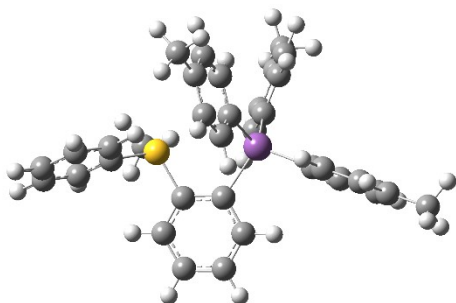


Sb	0.773347	-0.000667	-0.064134	C	-4.024545	0.370133	-0.480006
S	-2.418227	1.176068	-0.351093	C	0.938620	3.032664	0.367035
C	-0.276892	0.313469	-1.895920	H	0.871467	3.085603	-0.715428
C	-2.272950	0.934706	-3.131710	C	-1.561932	-2.700601	2.534020
H	-3.300430	1.279805	-3.142765	H	-2.568207	-2.727481	2.940578
C	0.107828	-1.595927	1.167693	C	1.050518	4.214308	1.104166
C	2.747602	-0.513687	-0.643870	H	1.075805	5.166187	0.582920
C	0.907335	1.795982	1.036391	C	-4.144846	-1.007528	-0.730137
C	-1.617864	0.757020	-1.902012	H	-3.259730	-1.612538	-0.894615
C	-0.269763	0.256679	-4.324345	C	5.398350	-1.166485	-1.389198
H	0.250055	0.066439	-5.256629	C	-1.071993	-4.875089	3.747594
C	-0.654785	-3.724476	2.863298	H	-1.492356	-5.694809	3.149719
C	0.398650	0.083944	-3.108316	H	-1.838697	-4.570906	4.466665
H	1.433915	-0.238081	-3.109271	H	-0.222752	-5.281555	4.305082
C	-1.606548	0.672874	-4.332089	C	1.096013	2.945349	3.160769
H	-2.127527	0.809300	-5.273543	H	1.157664	2.907689	4.243905
C	-1.194727	-1.644192	1.696778	C	-5.170522	1.150385	-0.259094
H	-1.915922	-0.870571	1.464427	H	-5.073823	2.214782	-0.074326
C	3.013544	-1.697898	-1.360703	C	6.809423	-1.502246	-1.809618
H	2.212933	-2.380146	-1.631820	H	6.973273	-2.583892	-1.839151
C	3.811557	0.338735	-0.299445	H	7.545644	-1.063891	-1.129387
H	3.631882	1.252700	0.257241	H	7.020645	-1.113196	-2.814594
C	4.325113	-2.013506	-1.724519	C	-5.413071	-1.594306	-0.773228
H	4.519545	-2.930297	-2.272599	H	-5.506489	-2.656106	-0.975816
C	1.031286	-2.607239	1.492961	C	-6.558404	-0.819037	-0.546728
H	2.044117	-2.583915	1.106786	H	-7.539662	-1.280259	-0.575235
C	5.118700	0.008609	-0.669683	C	-6.435148	0.549851	-0.285522
H	5.932688	0.671737	-0.393830	H	-7.319177	1.154300	-0.113302
C	0.645448	-3.655759	2.332488	C	1.216431	5.476079	3.299136
H	1.366364	-4.428349	2.581294	H	1.724183	6.262239	2.732122
C	0.984861	1.753860	2.439366	H	1.755100	5.331709	4.240533
H	0.954820	0.808348	2.971841	H	0.214773	5.849825	3.550075
C	1.127855	4.192040	2.509024				

Table S3. XYZ coordinates of the optimized geometry of $[3]^{2+}$.

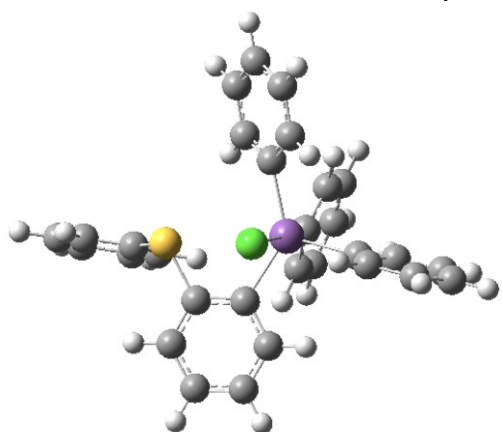


Sb	-1.204009	-0.133473	-0.074696	H	-6.373392	-1.938600	2.338820
S	2.191307	0.974746	-0.209572	C	-2.255444	3.690565	-2.967532
C	-1.597639	1.505060	-1.350454	H	-2.513835	4.537199	-3.593565
C	-0.205553	-1.730817	-1.038145	C	1.504596	1.419675	3.804496
C	0.039803	0.588837	1.531659	H	2.071358	1.729292	4.674942
C	-3.008273	-0.788944	0.801657	C	3.930416	-1.109402	-0.346970
C	1.392777	0.993776	1.422136	H	3.069665	-1.666217	-0.701288
C	-3.985867	0.170872	1.130968	C	-4.457839	-2.566266	1.574131
H	-3.825129	1.228177	0.943941	H	-4.647392	-3.621143	1.737687
C	-1.344243	2.814033	-0.894974	C	-2.517678	2.388362	-3.412476
H	-0.924438	2.992766	0.090806	H	-2.980283	2.226449	-4.379589
C	-5.196821	-0.252465	1.689179	C	0.165557	1.038766	3.930562
H	-5.956566	0.478818	1.941211	H	-0.315972	1.053847	4.901711
C	0.207958	-2.837808	-0.269786	C	-0.558500	0.623870	2.804754
H	0.057690	-2.867865	0.805292	H	-1.592143	0.318453	2.927131
C	-2.196759	1.289595	-2.606604	C	0.621905	-2.799220	-3.050149
H	-2.431580	0.289691	-2.957288	H	0.778460	-2.788329	-4.123071
C	3.824688	0.251065	-0.011403	C	4.937118	0.991718	0.421284
C	-3.240167	-2.160226	1.016820	H	4.868818	2.047431	0.656463
H	-2.503357	-2.907723	0.743524	C	6.291009	-1.013065	0.206983
C	2.121485	1.395899	2.548417	H	7.254252	-1.503502	0.288964
H	3.166900	1.670321	2.462911	C	5.174076	-1.737296	-0.227989
C	0.005131	-1.706261	-2.429217	H	5.271160	-2.785520	-0.485638
H	-0.300041	-0.856202	-3.029747	C	6.173346	0.346674	0.525839
C	1.026365	-3.905619	-2.291561	H	7.042031	0.907810	0.850489
H	1.492407	-4.754008	-2.780307	C	2.494783	2.743688	-0.563179
C	-1.676061	3.903774	-1.709867	H	2.955925	3.246021	0.287221
H	-1.497737	4.914156	-1.358053	H	1.524574	3.190833	-0.786673
C	0.823958	-3.923440	-0.904590	H	3.138169	2.796472	-1.4440
H	1.133517	-4.782442	-0.319377				
C	-5.430714	-1.616231	1.911037				

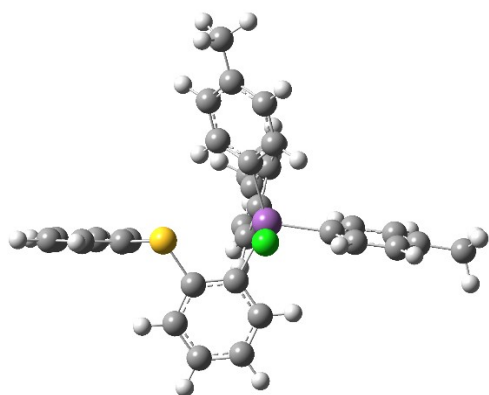
Table S4. XYZ coordinates of the optimized geometry of [4]²⁺

Sb	-0.994974	-0.107725	-0.043191	C	-4.228397	-2.923968	0.857784
S	2.351672	1.100069	0.271113	H	-4.379086	-3.995446	0.775734
C	-1.372493	1.739584	-0.989256	C	-2.197962	2.997451	-2.891475
C	0.124870	-1.442344	-1.236355	H	-2.592707	3.013424	-3.902300
C	0.118782	0.324381	1.755458	C	0.075820	0.313869	4.199029
C	-2.807668	-0.984897	0.570065	H	-0.463886	0.125398	5.120160
C	1.453755	0.791389	1.818799	C	-0.556396	0.093643	2.968089
C	-3.839090	-0.155722	1.054271	H	-1.578823	-0.268424	2.957334
H	-3.714046	0.921044	1.119478	C	1.127972	-2.047574	-3.359374
C	-1.197805	2.941837	-0.277385	H	1.357598	-1.798726	-4.390500
H	-0.845058	2.938809	0.750157	C	5.052536	1.078626	1.073038
C	-5.053615	-0.725805	1.441216	H	4.933186	2.078822	1.472467
H	-5.846694	-0.085195	1.812833	C	6.485213	-0.830333	0.625793
C	0.530584	-2.679338	-0.696678	H	7.457525	-1.305104	0.691487
H	0.315273	-2.944500	0.334328	C	5.422836	-1.498678	0.004518
C	-1.887547	1.770991	-2.300400	H	5.571379	-2.487840	-0.412736
H	-2.063032	0.857480	-2.859792	C	6.301440	0.454787	1.153553
C	3.995352	0.393986	0.451837	H	7.128311	0.974924	1.623274
C	-3.005242	-2.374689	0.467498	C	2.611412	2.910431	0.269175
H	-2.231537	-3.027175	0.077324	H	2.995058	3.259497	1.228000
C	2.092156	1.000464	3.047817	H	1.642109	3.366254	0.059574
H	3.126304	1.323510	3.087775	H	3.309889	3.140264	-0.538281
C	0.433262	-1.125179	-2.572604	C	-2.391114	5.525296	-2.840971
H	0.144491	-0.173279	-3.005526	H	-2.068520	5.565229	-3.886397
C	1.527133	-3.296597	-2.844120	H	-3.479755	5.666427	-2.834980
C	-1.518313	4.160632	-0.884657	H	-1.947492	6.373593	-2.313298
H	-1.393045	5.083490	-0.327104	C	-6.598714	-2.716585	1.736769
C	1.226360	-3.588959	-1.499030	H	-7.106963	-2.116463	2.496730
H	1.528981	-4.543316	-1.079860	H	-7.266106	-2.774305	0.866537
C	-5.271489	-2.114661	1.348822	H	-6.482027	-3.733262	2.123203
C	-2.020634	4.211845	-2.198634	C	2.232805	-4.303081	-3.718583
C	1.398845	0.763544	4.240003	H	2.836799	-4.999242	-3.129908
H	1.894722	0.924205	5.190296	H	1.504176	-4.901188	-4.281650
C	4.168164	-0.889336	-0.093716	H	2.883090	-3.815712	-4.451
H	3.349915	-1.400353	-0.589912				

Table S5. XYZ coordinates of the optimized geometry of **1-Cl**.

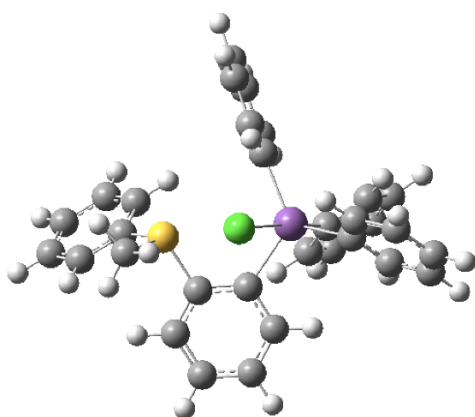


Sb	-0.998696	0.016131	-0.287139	H	-3.613420	-0.799203	-1.953221
Cl	-1.427742	-0.055149	-2.882095	C	-5.202407	-1.402671	-0.622588
S	2.262285	0.147448	-1.404071	H	-5.900483	-1.597273	-1.430755
C	-0.919218	2.151797	-0.575135	C	-5.590974	-1.605286	0.706290
C	-1.990265	2.791767	-1.217604	H	-6.592507	-1.956829	0.934198
H	-2.809563	2.213133	-1.627657	C	-4.682994	-1.354305	1.740725
C	-1.982794	4.184510	-1.360123	H	-4.975411	-1.510249	2.774504
H	-2.813937	4.676680	-1.855020	C	0.273131	-1.664092	-0.757152
C	-0.903247	4.936288	-0.881249	C	1.618474	-1.507644	-1.137910
H	-0.895376	6.014818	-1.003823	C	2.404099	-2.645654	-1.389732
C	0.168821	4.295032	-0.250543	H	3.437873	-2.523689	-1.693898
H	1.012161	4.872336	0.115354	C	1.856539	-3.923801	-1.255522
C	0.160339	2.903529	-0.088239	H	2.473631	-4.795439	-1.448341
H	0.992425	2.416857	0.407422	C	0.511853	-4.078935	-0.896959
C	0.372573	-0.946199	2.411146	H	0.079922	-5.070288	-0.806963
H	0.646218	-1.814976	1.821972	C	-0.280237	-2.951049	-0.656206
C	-0.344046	0.112565	1.819086	H	-1.323518	-3.076984	-0.384812
C	-0.693075	1.213126	2.628225	C	3.918934	-0.162553	0.845611
H	-1.246077	2.046225	2.206660	H	3.022600	-0.414958	1.401229
C	-0.331225	1.257549	3.980761	C	3.835398	0.124282	-0.527991
H	-0.609679	2.115784	4.585047	C	4.995498	0.473984	-1.238445
C	0.387962	0.200749	4.551313	H	4.928831	0.690008	-2.299413
H	0.670402	0.235562	5.598983	C	6.229403	0.537131	-0.579415
C	0.737772	-0.902007	3.764180	H	7.121267	0.809679	-1.134694
H	1.289618	-1.729495	4.200522	C	6.313662	0.238248	0.784570
C	-3.390882	-0.899924	1.449902	H	7.271347	0.281176	1.293337
H	-2.702199	-0.710115	2.263737	C	5.157073	-0.114491	1.493064
C	-2.996863	-0.692413	0.113959	H	5.216275	-0.340412	2.553165
C	-3.911945	-0.948973	-0.922798				

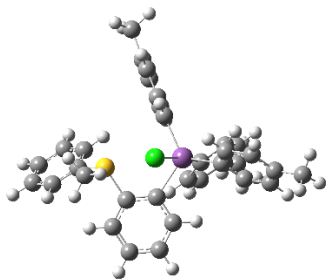
Table S6. XYZ coordinates of the optimized geometry of [2-Cl]

Sb	-0.823660	0.066972	-0.444733	C	0.331184	-1.531321	-1.324928
Cl	-1.250728	0.644535	-2.983545	C	1.686897	-1.386819	-1.672669
S	2.456904	0.230286	-1.538056	C	2.387477	-2.484364	-2.202486
C	-0.571711	2.193027	-0.218944	H	3.429194	-2.368111	-2.480754
C	-1.561175	3.060872	-0.705946	C	1.746531	-3.713407	-2.375191
H	-2.410546	2.671866	-1.254872	H	2.298694	-4.554951	-2.781080
C	-1.437229	4.439349	-0.509936	C	0.392019	-3.851868	-2.048210
H	-2.212581	5.101441	-0.885303	H	-0.112769	-4.801058	-2.195770
C	-0.321599	4.983465	0.150330	C	-0.315528	-2.760977	-1.532040
C	0.663102	4.102358	0.625873	H	-1.367047	-2.871764	-1.287063
H	1.534898	4.499773	1.138290	C	4.070620	-0.744942	0.546428
C	0.541346	2.718830	0.451804	H	3.153789	-1.056188	1.034736
H	1.314448	2.063560	0.836322	C	4.018100	-0.125349	-0.714371
C	0.472810	-1.606110	1.923989	C	5.206491	0.298218	-1.331843
H	0.700082	-2.322161	1.141218	H	5.163606	0.771474	-2.307023
C	-0.176587	-0.397131	1.609927	C	6.437306	0.104193	-0.692817
C	-0.468091	0.483262	2.671787	H	7.351101	0.435624	-1.175773
H	-0.973004	1.424074	2.477002	C	6.489546	-0.525120	0.555423
C	-0.116016	0.170174	3.988769	H	7.444407	-0.681306	1.047118
H	-0.356694	0.867711	4.787082	C	5.304533	-0.951329	1.170399
C	0.543784	-1.032095	4.297627	H	5.339262	-1.434000	2.142144
C	0.827170	-1.915624	3.243792	C	-6.969479	-1.890438	0.386923
H	1.324292	-2.858630	3.457104	H	-7.683701	-1.229839	-0.116807
C	-3.274971	-1.109414	1.030948	H	-7.113524	-2.898047	-0.026354
H	-2.573449	-1.203397	1.850691	H	-7.234472	-1.931025	1.448359
C	-2.866589	-0.573048	-0.204310	C	-0.174250	6.479517	0.316595
C	-3.809808	-0.463643	-1.241974	H	0.495782	6.726513	1.146571
H	-3.509834	-0.060010	-2.201401	H	0.243409	6.938538	-0.589797
C	-5.129079	-0.879727	-1.039892	H	-1.140983	6.959102	0.505879
H	-5.844568	-0.783257	-1.852077	C	0.951420	-1.352634	5.718556
C	-5.546458	-1.418479	0.189252	H	0.206905	-0.996656	6.439273
C	-4.597806	-1.524305	1.218861	H	1.077077	-2.430398	5.865508
H	-4.894923	-1.933333	2.180703	H	1.905953	-0.873512	5.976257

Table S7. XYZ coordinates of the optimized geometry of [3-Cl]⁺



Sb	1.102936	0.024774	-0.205934	C	-0.296910	3.383574	2.268255
S	-2.359084	0.798629	-0.927040	H	0.204489	4.005883	3.001174
C	1.411816	-1.023135	1.683082	C	0.404949	2.346567	1.643974
C	-0.206946	1.531222	0.674295	H	1.441798	2.179193	1.914589
C	3.125773	0.673292	-0.485097	Cl	0.483418	1.472020	-2.393326
C	-1.554319	1.793738	0.359160	C	0.336818	-1.692128	-1.259199
C	3.928553	0.850143	0.656809	C	-0.152796	-2.768630	-0.495163
H	3.541211	0.648960	1.648919	C	0.368846	-1.781862	-2.660440
C	0.546993	-0.883604	2.784578	C	-0.621046	-3.922178	-1.138405
H	-0.279492	-0.181488	2.752524	H	-0.151976	-2.728276	0.587675
C	5.256112	1.271730	0.513211	C	-0.083703	-2.947687	-3.290703
H	5.870256	1.416978	1.395623	H	0.725287	-0.951069	-3.255246
C	2.470641	-1.951397	1.768272	C	-0.583138	-4.014487	-2.534329
H	3.153801	-2.085593	0.934616	H	-0.996867	-4.750242	-0.546221
C	-2.897786	2.029798	-2.162327	H	-0.044027	-3.018299	-4.372521
C	3.655316	0.908179	-1.764218	H	-0.934199	-4.913949	-3.028979
H	3.035870	0.805640	-2.645634	H	-1.981918	2.364733	-2.651524
C	-2.273484	2.812278	1.000294	H	-3.545259	1.515061	-2.874910
H	-3.320058	2.981063	0.774327	H	-3.415537	2.866213	-1.693400
C	0.741478	-1.644023	3.946406	C	-3.897611	0.203090	-0.195787
H	0.069095	-1.521486	4.789565	C	-3.860230	-1.120077	0.273533
C	5.788035	1.496384	-0.761134	C	-5.071258	0.967462	-0.113623
H	6.818784	1.816507	-0.869821	C	-5.007419	-1.671329	0.853071
C	1.800280	-2.555090	4.020453	H	-2.958202	-1.715152	0.172600
H	1.952184	-3.141086	4.920734	C	-6.212705	0.399539	0.461340
C	-1.640395	3.612235	1.954338	H	-5.119182	1.978669	-0.499787
H	-2.193106	4.404949	2.445278	C	-6.180149	-0.913240	0.948838
C	4.989671	1.309222	-1.895838	H	-4.986176	-2.692461	1.216413
H	5.399124	1.482938	-2.885080	H	-7.125433	0.981418	0.523225
C	2.664618	-2.708592	2.928871	H	-7.069871	-1.346219	1.392119
H	3.486898	-3.414718	2.980436				

Table S8. XYZ coordinates of the optimized geometry of [4-Cl]⁺

Sb	-0.900802	-0.170708	-0.233139	C	0.591854	2.394684	-1.031200
S	2.503787	-1.342069	-0.605580	C	0.091408	1.011003	-2.963615
C	-1.185611	1.261074	1.382109	C	1.181049	3.345220	-1.873307
C	0.246084	-1.556336	1.002120	H	0.544567	2.590112	0.033762
C	-2.951955	-0.716087	-0.486741	C	0.666103	1.979078	-3.791870
C	1.576254	-1.979773	0.817692	H	-0.301385	0.099703	-3.395537
C	-3.818536	-0.583141	0.612272	C	1.221098	3.159869	-3.265563
H	-3.462563	-0.199910	1.561732	H	1.599005	4.250219	-1.442042
C	-0.374318	1.295621	2.530229	H	0.683652	1.813022	-4.864945
H	0.395985	0.547433	2.686018	H	2.070507	-3.212062	-1.976456
C	-5.168515	-0.926525	0.480946	H	3.703589	-2.540677	-2.290145
H	-5.827559	-0.826520	1.337966	H	3.423358	-3.593811	-0.858232
C	-2.164138	2.266285	1.229876	C	4.056163	-0.712595	0.067007
H	-2.806742	2.280649	0.354236	C	4.105605	0.679627	0.244970
C	2.991051	-2.844261	-1.520680	C	5.161406	-1.520766	0.372819
C	-3.451979	-1.184365	-1.713369	C	5.269145	1.261221	0.758597
H	-2.793539	-1.320794	-2.561426	H	3.258172	1.300260	-0.028452
C	2.185541	-2.891341	1.691487	C	6.320834	-0.923625	0.878008
H	3.221218	-3.182275	1.558776	H	5.143774	-2.591990	0.211274
C	-0.544109	2.293241	3.499122	C	6.373339	0.461972	1.076444
H	0.093276	2.297831	4.378762	H	5.314451	2.335360	0.897908
C	-5.685715	-1.388830	-0.740073	H	7.181282	-1.540636	1.111391
C	-1.525662	3.286649	3.354821	H	7.276326	0.917012	1.467834
C	1.455347	-3.422763	2.756943	C	-7.140992	-1.769582	-0.878525
H	1.922469	-4.133521	3.428946	H	-7.575458	-1.358861	-1.796579
C	-4.806129	-1.503536	-1.832743	H	-7.258982	-2.859985	-0.925628
H	-5.183920	-1.855217	-2.788060	H	-7.733057	-1.409449	-0.032323
C	-2.330141	3.257267	2.200018	C	1.816584	4.208291	-4.175765
H	-3.092176	4.018754	2.060606	H	2.366958	3.753490	-5.006082
C	0.125715	-3.033259	2.947534	H	1.030449	4.836375	-4.615203
H	-0.450912	-3.448207	3.766822	H	2.499616	4.870364	-3.635155
C	-0.464746	-2.101261	2.087204	C	-1.728818	4.346939	4.412285
H	-1.492430	-1.802784	2.263531	H	-2.607919	4.123417	5.030946
Cl	-0.314759	-2.101407	-2.042876	H	-0.866112	4.417311	5.081450
C	0.048182	1.215907	-1.574383	H	-1.893069	5.333123	3.964533

Natural bond orbital (NBO) analysis

The optimized structures were also subjected to NBO analysis. The molecular orbitals and NBOs were visualized and plotted using the Avogadro program.⁹

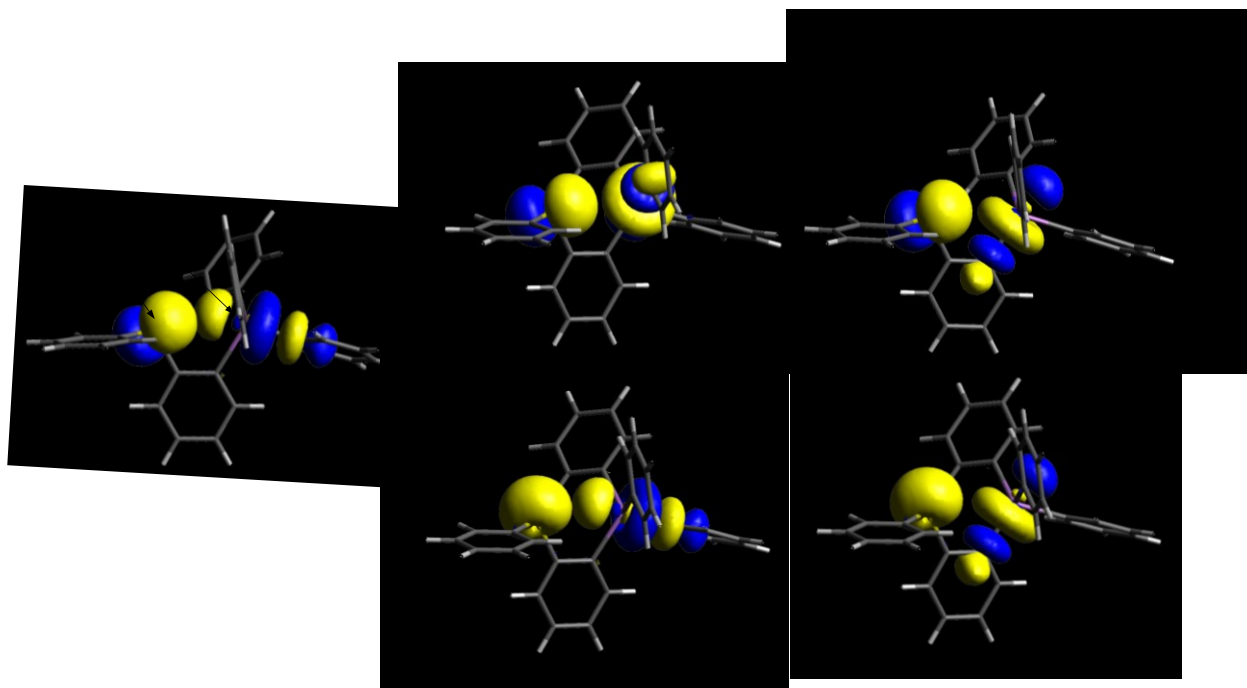


Figure S23. Donor-acceptor interactions (isovalue = 0.05) present in $[1]^+$. All $\text{lp}(\text{S}) \rightarrow \sigma^*(\text{Sb-C})$ donor-acceptor interactions contribute $E_{\text{del}} = 6.82$ kcal/mol to the stability of the compound.

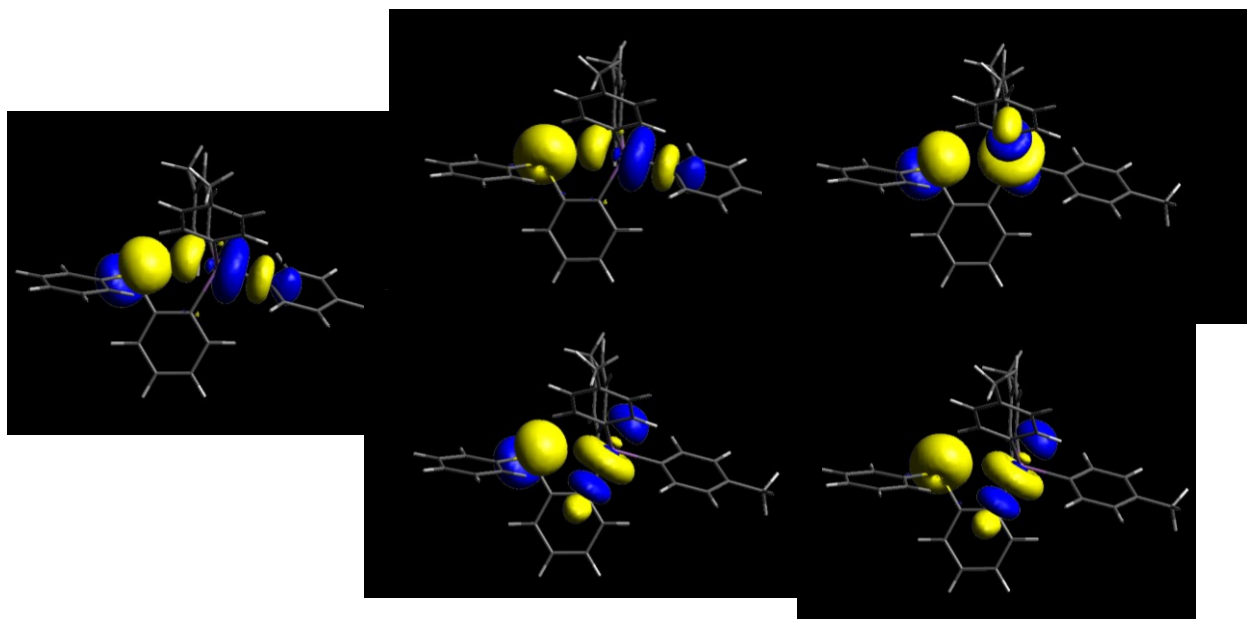


Figure S24. Donor-acceptor interactions (isovalue = 0.05) present in $[2]^+$. All $\text{lp}(\text{S}) \rightarrow \sigma^*(\text{Sb-C})$ donor-acceptor interactions contribute $E_{\text{del}} = 6.67$ kcal/mol to the stability of the compound.

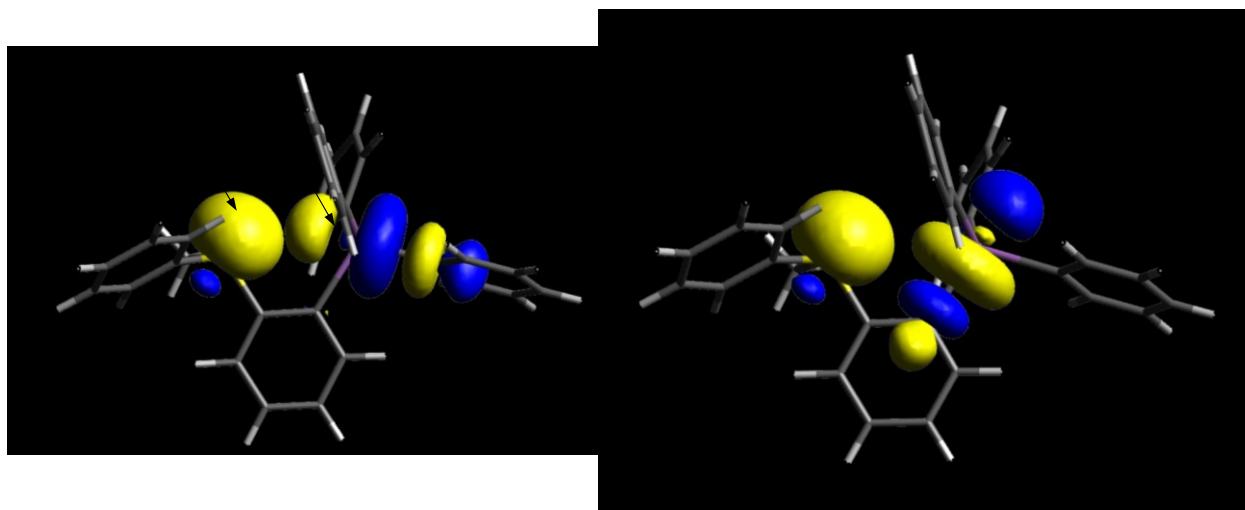


Figure S25. Donor-acceptor interactions (isovalue = 0.05) present in $[3]^{2+}$. All $lp(S) \rightarrow \sigma^*(Sb-C)$ donor-acceptor interactions contribute $E_{del} = 2.42$ kcal/mol to the stability of the compound.

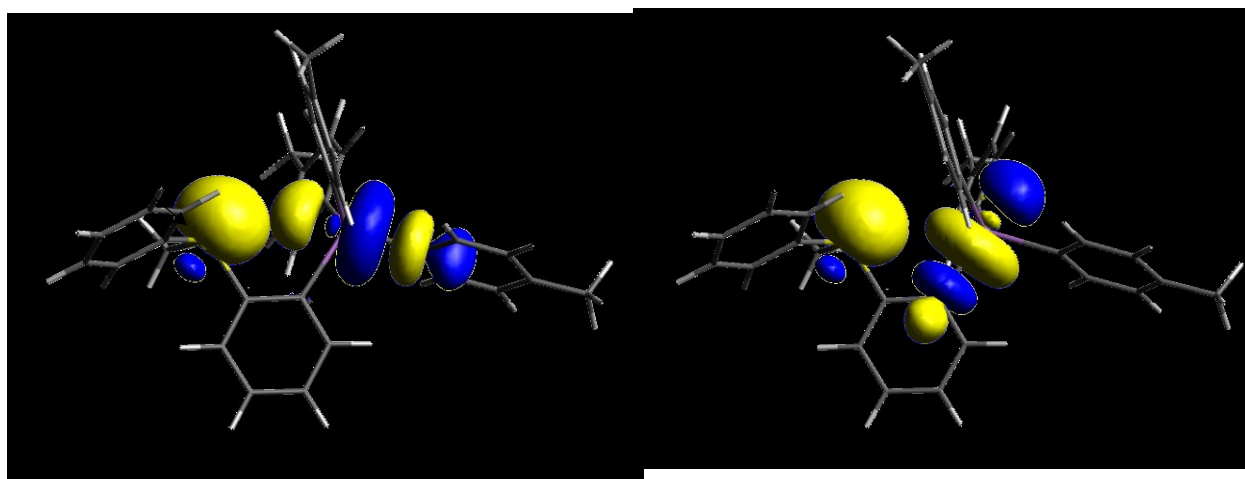


Figure S26. Donor-acceptor interactions (isovalue = 0.05) present in $[4]^{2+}$. All $lp(S) \rightarrow \sigma^*(Sb-C)$ donor-acceptor interactions contribute $E_{del} = 2.39$ kcal/mol to the stability of the compound.

Electrostatic potential surface (ESPs) and distribution of the electrostatic potential on the molecular surfaces (V_S)

Electrostatic potential surfaces (ESPs) were created based on the optimized structures and determined at an isodensity value of 0.001 electrons/Bohr³. ESP maps were generated and analyzed using the Mutliwfn program¹⁰ and visualized using VMD.¹¹ The Mutliwfn program was also used to identify the positions of maximum electrostatic potential ($V_{S, max}$).

Partition coefficients:

Using a published approach^{12, 13} illustrated in Figure S27, the solute electron density-based implicit solvation model (SMD)¹⁴ was used to estimate the solvation of free energy of stibonium cations in water (ΔG_w) and in n-octanol (ΔG_o). Only the gas phase structures were optimized. The energies of the solvated molecule were obtained via single point calculations. The octanol-water partition coefficient K_{ow} was calculated based on the following equation with $T = 298$ K.¹⁵ The calculation results are presented in Table S9.

$$\log K_{ow} = \frac{-\Delta G_{ow}}{2.303RT} = \frac{\Delta G_w - \Delta G_o}{2.303RT}$$

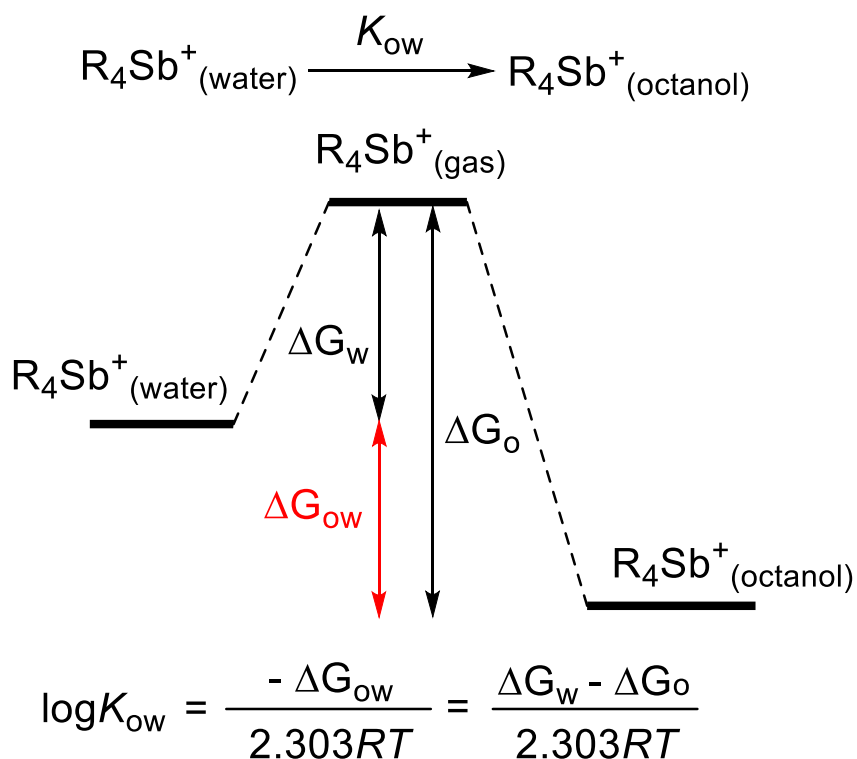


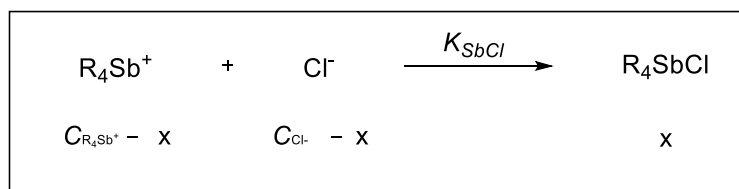
Figure S27. Diagram representing the approach adopted to determine the partition coefficient K_{ow} .

Table S9. Computed solvation energies and octanol-water partition coefficients

Compound	ΔG_w, Hartree (Kcal/mol)	ΔG_o, Hartree (Kcal/mol)	$-\Delta G_{ow}$, Kcal/mol	$\log K_{ow}$
[1] ⁺	-0.0589558 (-36.9952637)	-0.0722503 (-45.3376820)	8.3424184	6.1161425
[2] ⁺	-0.0525247 (-32.9597220)	-0.0692130 (-43.4317679)	10.472046	7.6774530
[3] ²⁺	-0.2128152 (-133.5434471)	-0.2118192 (-132.9184230)	-0.6250241	-0.4582288
[4] ²⁺	-0.2028079 (-127.2638139)	-0.2055625 (-128.99232)	1.7285050	1.2672323

Chloride anion binding experiments monitored by UV-vis spectroscopy in acetonitrile

Stibonium cations ($[1]^+$, $[2]^+$, $[3]^{2+}$ and $[4]^{2+}$) (0.005 mmol) were dissolved in acetonitrile (1 mL). 30 μ L of the resulting acetonitrile solution was added to an acetonitrile solution (2.970 mL) resulting in a $5 \cdot 10^{-5}$ M solution of the stibonium cations. Aliquots (1.25-40 μ L) of TBACl solution ($[TBACl] = 10$ mM or $[TBACl] = 100$ mM) were incrementally added to the solution containing the cations. After each addition, the solution was stirred, and its UV-vis spectra was recorded at room temperature. The resulting absorbance data were fitted to the calculated absorbance obtained with the following equations to provide the chloride binding constant. The fitting was carried out by hand using Excel.



$$K_{SbCl} = \frac{[R_4SbCl]}{[R_4Sb^+][Cl^-]} = \frac{x}{(C_{R_4Sb^+} - x)(C_{Cl^-} - x)}$$

$$\Rightarrow x^2 - x \cdot (C_{R_4Sb^+} + C_{Cl^-} + 1/K_{SbCl}) + C_{R_4Sb^+} \cdot C_{Cl^-}$$

$$\Rightarrow x = \frac{C_{R_4Sb^+} + C_{Cl^-} + 1/K_{SbCl} - \sqrt{(C_{R_4Sb^+} + C_{Cl^-} + 1/K_{SbCl})^2 - 4 C_{R_4Sb^+} \cdot C_{Cl^-}}}{2} \dots\dots\dots (1)$$

$$A = \varepsilon \cdot b \cdot c$$

$$A_{Cal.} = \varepsilon_{R_4SbCl} \cdot b \cdot [R_4SbCl] + \varepsilon_{R_4Sb^+} \cdot b \cdot [R_4Sb^+]$$

$$= \varepsilon_{R_4SbCl} \cdot b \cdot x + \varepsilon_{R_4Sb^+} \cdot b \cdot (C_{R_4Sb^+} - x) \dots\dots\dots (2)$$

with :

- $C_{R_4Sb^+}$ = molar concentration of the stibonium solution (mol/L)
- C_{Cl^-} = initial molar concentration of Cl^- anion solution (mol/L)
- x = initial molar concentration of stibonium chloride complex solution (mol/L)
- K_{SbCl} = chloride binding constant of the stibonium cation (M^{-1})
- A = absorbance
- ε = molar extinction coefficient
- b = width of the cuvette (1 cm)
- c = molar concentration (mol/L)
- $A_{Cal.}$ = calculated absorbance
- $\varepsilon_{R_4Sb^+}$ = molar extinction coefficient of the stibonium cation ($M^{-1}cm^{-1}$)

$\epsilon_{R,SbCl}$ = molar extinction coefficient of the stibonium chloride complex ($M^{-1}cm^{-1}$)

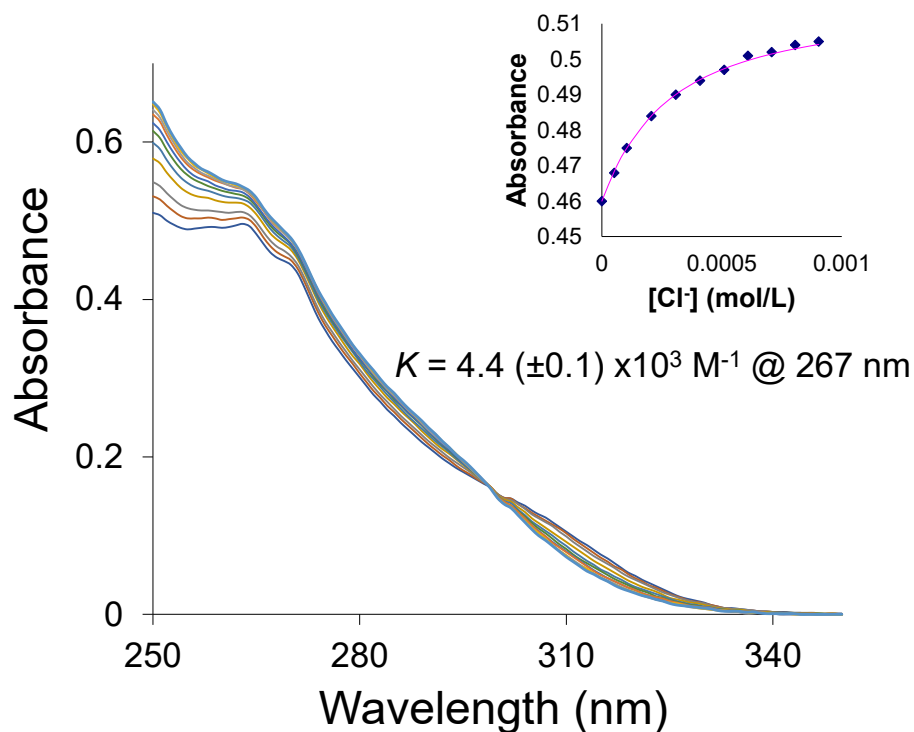


Figure S28. Changes observed in the absorption spectrum of $[1]^+$ in acetonitrile upon incremental addition of TBACl dissolved in MeCN. The inset shows a plot of the absorbance at 267 nm as a function of chloride concentration. This plot was fitted to a 1:1 binding model with $K = 4.4 (\pm 0.1) \times 10^3 M^{-1}$, $\epsilon([1]^+) = 7130 M^{-1} cm^{-1}$ and $\epsilon([1]-Cl) = 8010 M^{-1} cm^{-1}$.

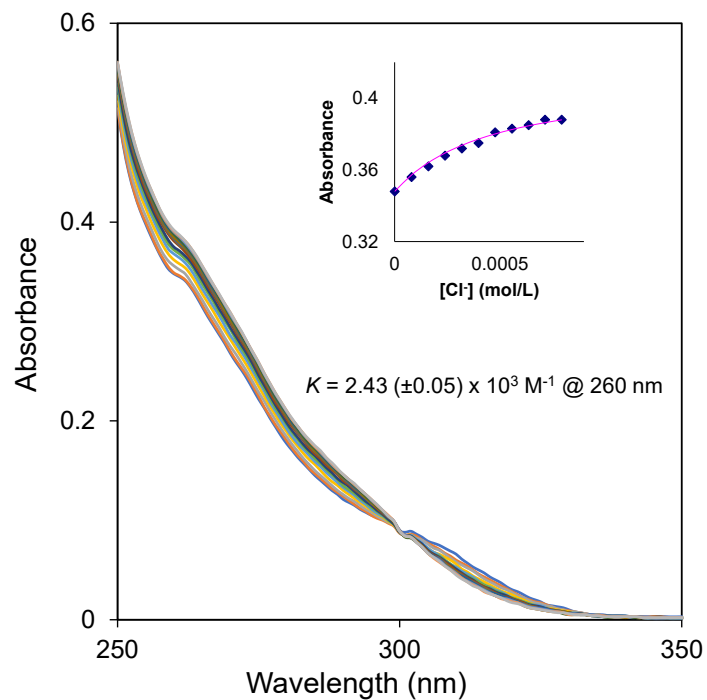


Figure S29. Changes observed in the absorption spectrum of $[2]^+$ in acetonitrile upon incremental addition of TBACl dissolved in MeCN. The inset shows a plot of the absorbance at 260 nm as a function of chloride concentration. This plot was fitted to a 1:1 binding model with $K = 2.43 (\pm 0.05) \times 10^3 \text{ M}^{-1}$, $\epsilon([2]^+) = 6960 \text{ M}^{-1} \text{ cm}^{-1}$ and $\epsilon([2]-\text{Cl}) = 8200 \text{ M}^{-1} \text{ cm}^{-1}$.

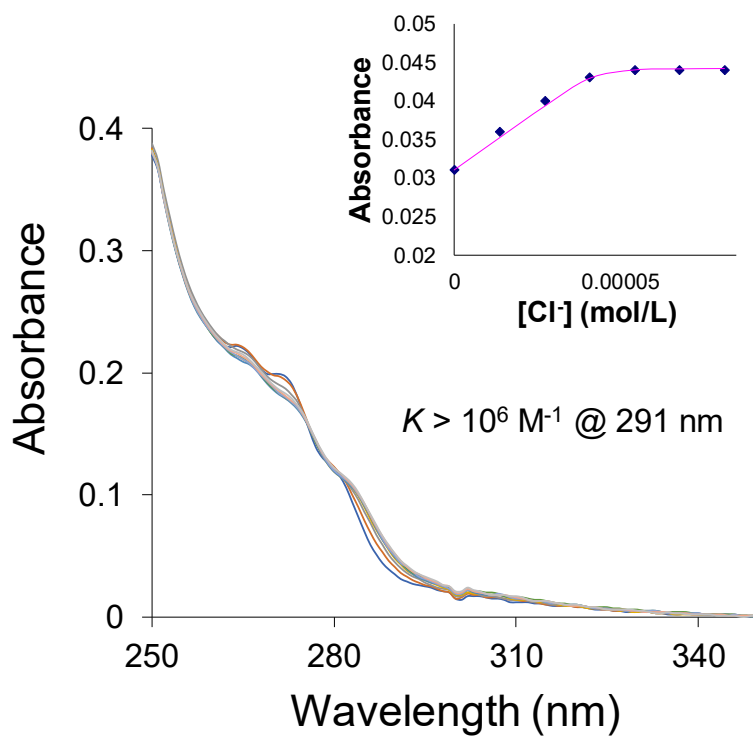


Figure S30. Changes observed in the absorption spectrum of $[\mathbf{3}]^{2+}$ in acetonitrile upon incremental addition of TBACl dissolved in MeCN. The inset shows a plot of the absorbance at 291 nm as a function of chloride concentration. This plot could be fitted for any values of K greater than 10^6 M^{-1} , $\epsilon([\mathbf{3}]^{2+}) = 721 \text{ M}^{-1} \text{ cm}^{-1}$ and $\epsilon([\mathbf{3}\text{-Cl}]^+) = 1030 \text{ M}^{-1} \text{ cm}^{-1}$.

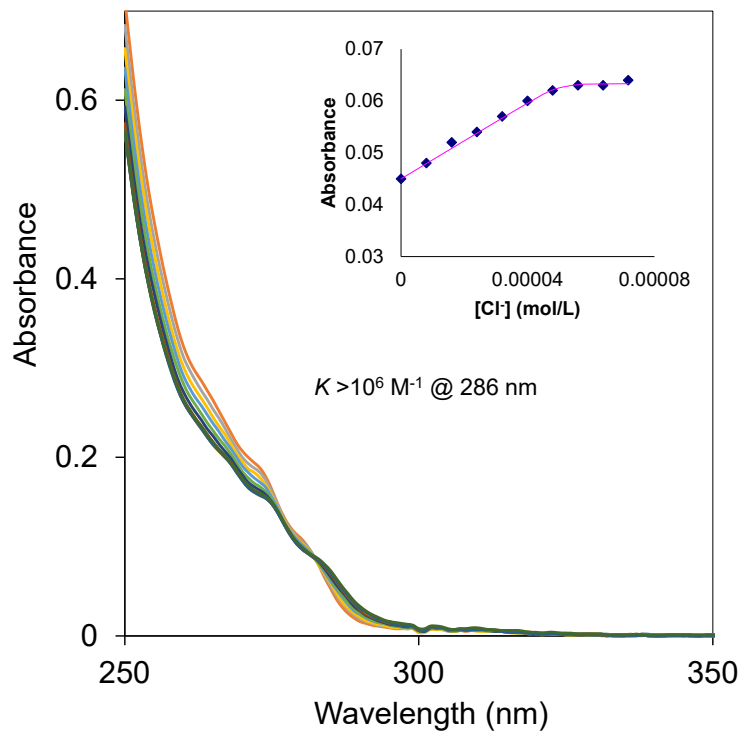


Figure S31. Changes observed in the absorption spectrum of $[4]^{2+}$ in acetonitrile upon incremental addition of TBACl dissolved in MeCN. The inset shows a plot of the absorbance at 286 nm as a function of chloride concentration. This plot could be fitted for any values of K greater than 10^6 M^{-1} , $\epsilon([4]^{2+}) = 900 \text{ M}^{-1} \text{ cm}^{-1}$ and $\epsilon([4-Cl]^+) = 1268 \text{ M}^{-1} \text{ cm}^{-1}$.

Vesicle Preparation

POPC-LUVs. The transport experiments were conducted using POPC large unilamellar vesicles (200 nm diameter) loaded with a chloride cargo. The vesicles were prepared according to a previously established method.¹⁶ A thin film of the lipid was prepared by evaporation of a solution of POPC (40 mg) dissolved in CHCl₃ (1.6 mL). This film was dried under vacuum overnight. A buffered KCl solution (1 mL, 10 mM HEPES, 300 mM KCl, pH 7.2) was then added, resulting in a suspension which was then subjected to nine freeze-thaw cycles (liquid N₂, 47 °C water bath), and extruded 33 times through a 200 nm polycarbonate membrane. To remove any extravesicular component, the vesicle suspension was passed through a size exclusion column (Sephadex G-50) using a buffer solution (10 mM HEPES, 300 mM KGlc, pH 7.2) as an eluent.

DPPC-LUVs. The transport experiments were conducted using DPPC large unilamellar vesicles (200 nm diameter) loaded with a chloride cargo. The vesicles were prepared according to a previously established method.¹⁷ A thin film of the lipid was prepared by evaporation of a solution of DPPC (30 mg) dissolved in CHCl₃ (1.2 mL). This film was dried under vacuum overnight. A buffered KCl solution (1 mL, 10 mM HEPES, 300 mM KCl, pH 7.2) was then added at 50 °C, resulting in a suspension which was then subjected to nine freeze-thaw cycles (liquid N₂, 50 °C water bath), and extruded 33 times through a 200 nm polycarbonate membrane at 50 °C. To remove any extravesicular component, the vesicle suspension was passed through a size exclusion column (Sephadex G-50) using a buffer solution (10 mM HEPES, 300 mM KGlc, pH 7.2) as an eluent.

POPC-LUVs loaded with CF. The transport experiments were conducted using POPC large unilamellar vesicles (200 nm diameter) loaded with a chloride cargo. The vesicles were prepared according to a previously established method.¹⁸ A thin film of the lipid was prepared by evaporation of a solution of POPC (40 mg) dissolved in CHCl₃ (1.6 mL). This film was dried under vacuum overnight. A buffered KCl solution (1 mL, 10 mM HEPES, 10 mM KCl, 50 mM Carboxyfluorescein (CF) pH 7.4) was then added, resulting in a suspension which was then subjected to nine freeze-thaw cycles (liquid N₂, 47 °C water bath), and extruded 33 times through a 200 nm polycarbonate membrane. To remove any extravesicular component, the vesicle suspension was passed through a size exclusion column (Sephadex G-50) using a buffer solution (10 mM HEPES, 100 mM KCl, pH 7.4) as an eluent.

Chloride efflux in the presence of valinomycin

Internal solution: KCl 300 mM, HEPES 10 mM, pH 7.2

External solution: KGlc 300 mM, HEPES 10 mM, pH 7.2

The following assay was adapted from a previous report.¹⁶ POPC vesicles containing KCl were suspended in the external solution (5 mL) such that the final lipid concentration was equal to 0.7 mM. After the electrode voltage had stabilized (~30 s), the measurement ($t = 0$ s) was initiated by recording the electrode potential. At $t = 0$ s, valinomycin dissolved in DMSO (0.7 mM) was added to the assay such that the final valinomycin concentration was 0.1 mol %. At $t = 30$ s, the cations ($[1]^+$, $[2]^+$, $[3]^{2+}$, $[4]^{2+}$, Ph_4Sb^+ and Ph_2S) were added to the assay such that the concentration of cations was 2 mol% in DMSO. At $t = 300$ s, 50 μL of a Triton X solution (10:1:0.1 H₂O:DMSO:Triton X (v/v/v)) was added to lyse the vesicles triggering complete release of the chloride cargo. The value corresponding to 100% chloride efflux was recorded at $t = 420$ s, 2 min. after lysing the vesicles.

Chloride efflux in the absence of valinomycin

Internal solution: KCl 300 mM, HEPES 10 mM, pH 7.2

External solution: KGlc 300 mM, HEPES 10 mM, pH 7.2

POPC vesicles containing KCl were suspended in the external solution (5 mL) such that the final lipid concentration was equal to 0.7 mM. After the electrode voltage had stabilized (~30 s), the measurement ($t = 0$ s) was initiated by recording the electrode potential. At $t = 30$ s, transporter $[2]^+$ was added to the assay such that the concentration of transporter was 1 mol% in DMSO. At $t = 300$ s, 50 μ L of a Triton X solution (10:1:0.1 H₂O:DMSO:Triton X (v/v/v)) was added to lyse the vesicles triggering complete release of the chloride cargo. The value corresponding to 100% chloride efflux was recorded at $t = 420$ s, 2 min. after lysing the vesicles.

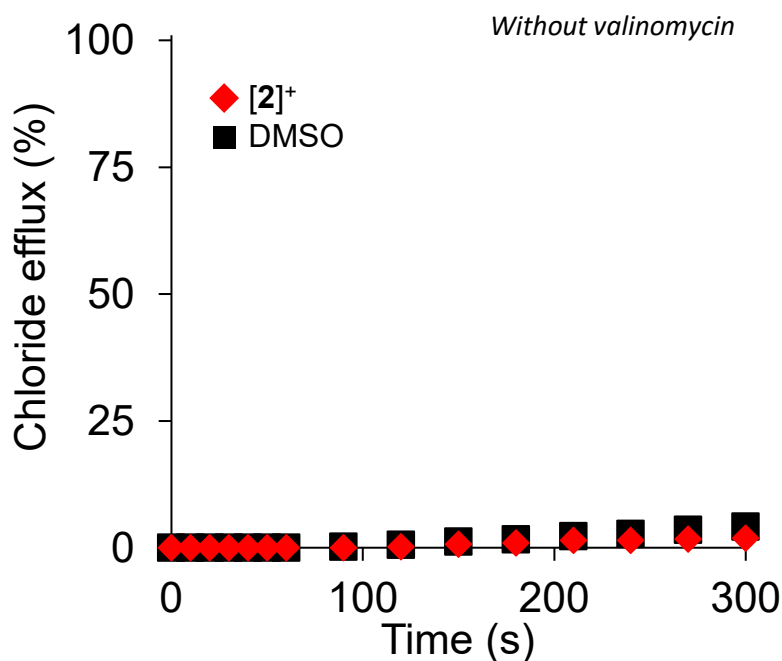


Figure S32. Chloride efflux from POPC vesicles triggered by addition of a DMSO solution (7 μ L) containing $[2]^+$ (1 mol% in DMSO with respect to the lipid concentration) in the absence of valinomycin. POPC concentration: 0.7 mM.

Initial rate of chloride efflux in the presence of valinomycin

The initial rate of chloride efflux (k_{ini}) was obtained by nonlinear fitting analysis of the experimentally measured chloride efflux (%) versus time (s), with the following asymptotic function¹⁹ using Origin Student 2020b:

$$y = a - b \cdot c^{(x-30)}$$

y is the chloride efflux (%)

x is time (s).

k_{ini} is then derived from $k_{ini} = -b \cdot \ln(c)$ ($\% \cdot s^{-1}$)

The data points before the addition of transporters were omitted from the fit. Since the addition of transporters occurs at $t = 30$ s, we modified the function above.

For compound with a low activity ($[3]^{2+}$ and $[4]^{2+}$), the initial rate of chloride efflux (k_{ini}) was obtained by fitting analysis of the experimentally measured chloride efflux (%) versus time (s), with the following asymptotic function¹⁹ using Origin Student 2020b:

$$y = a + b \cdot x$$

y is the chloride efflux (%)

x is time (s).

k_{ini} is then derived from $k_{ini} = \text{the slope } b$ ($\% \cdot s^{-1}$)

The data points used were those obtained between $t = 40$ s and 300 s.

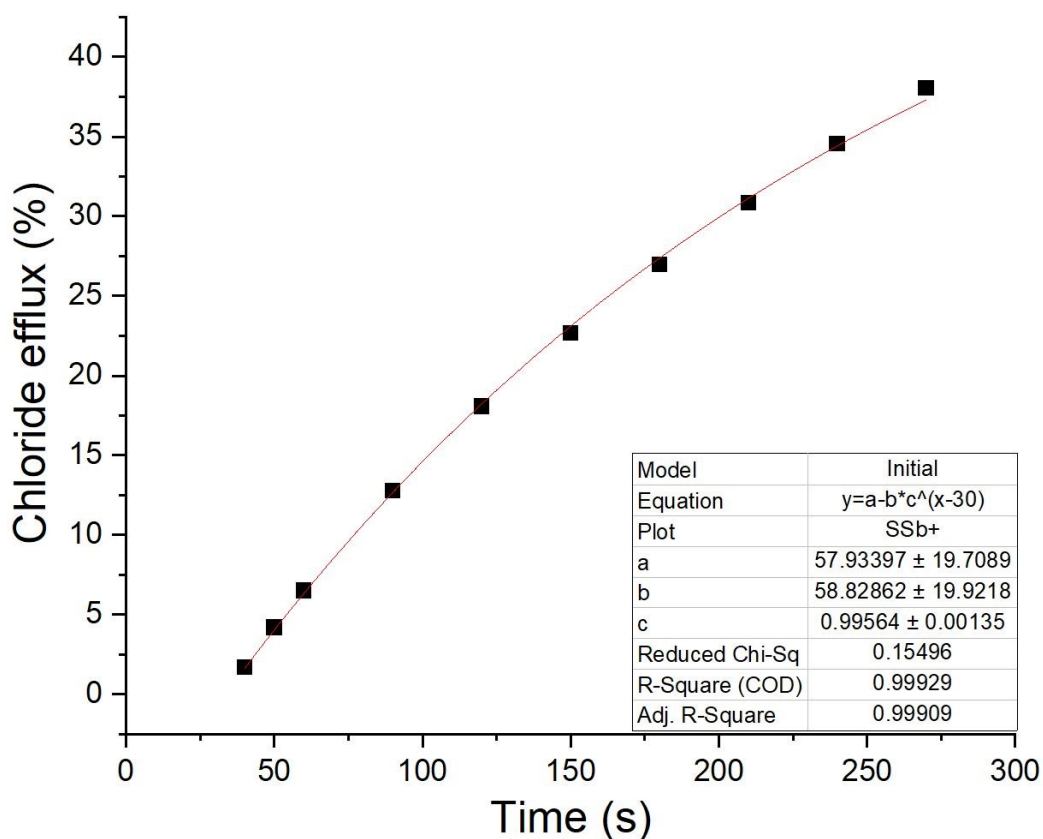


Figure S33. Kinetic fit of the valinomycin-coupled chloride efflux data observed when POPC vesicles are treated with $[1]^+$ as a transporter (2.0 mol% with respect to the lipid concentration). The POPC vesicles were loaded with KCl (300 mM) and suspended in KGlc (300 mM) buffered to pH 7.2. Each data point represents the average of three repeat measurements. $k_{ini.} = -b \cdot \ln(c) = 0.26 \% \cdot s^{-1}$.

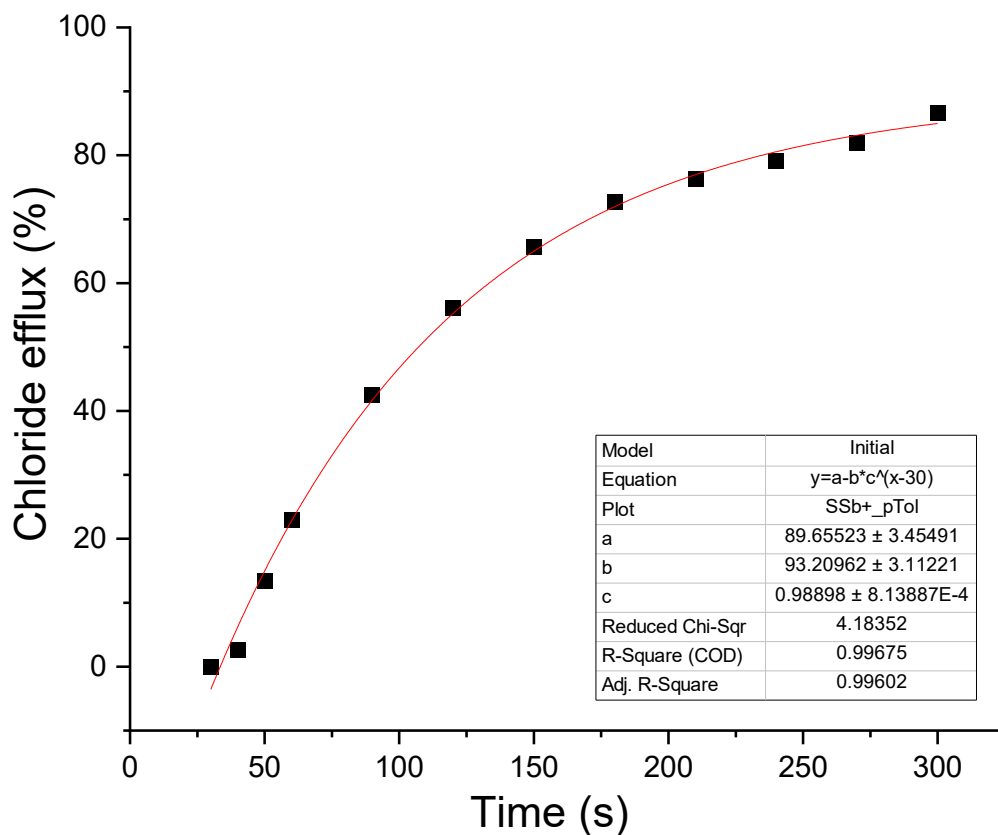


Figure S34. Kinetic fit of the valinomycin-coupled chloride efflux data observed when POPC vesicles are treated with $[2]^+$ as a transporter (2.0 mol% with respect to the lipid concentration). The POPC vesicles were loaded with KCl (300 mM) and suspended in KGlc (300 mM) buffered to pH 7.2. Each data point represents the average of three repeat measurements. $k_{ini.} = -b \cdot \ln(c) = 1.03 \% \cdot s^{-1}$.

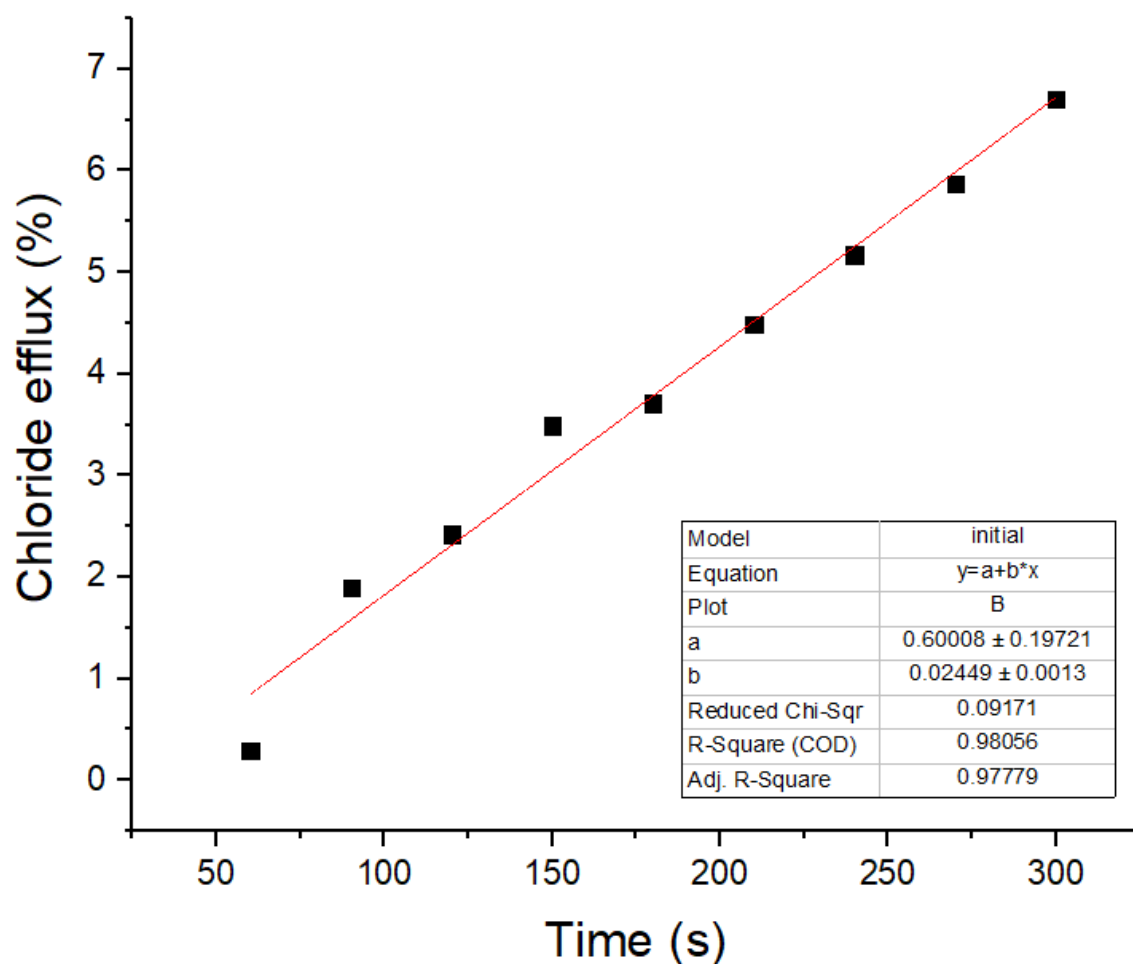


Figure S35. Kinetic fit of the valinomycin-coupled chloride efflux data observed when POPC vesicles are treated with $[3]^{2+}$ as a transporter (2.0 mol% with respect to the lipid concentration). The POPC vesicles were loaded with KCl (300 mM) and suspended in KGlc (300 mM) buffered to pH 7.2. Each data point represents the average of three repeat measurements. $k_{ini.} = b = 0.02 \text{ \%}\cdot\text{s}^{-1}$.

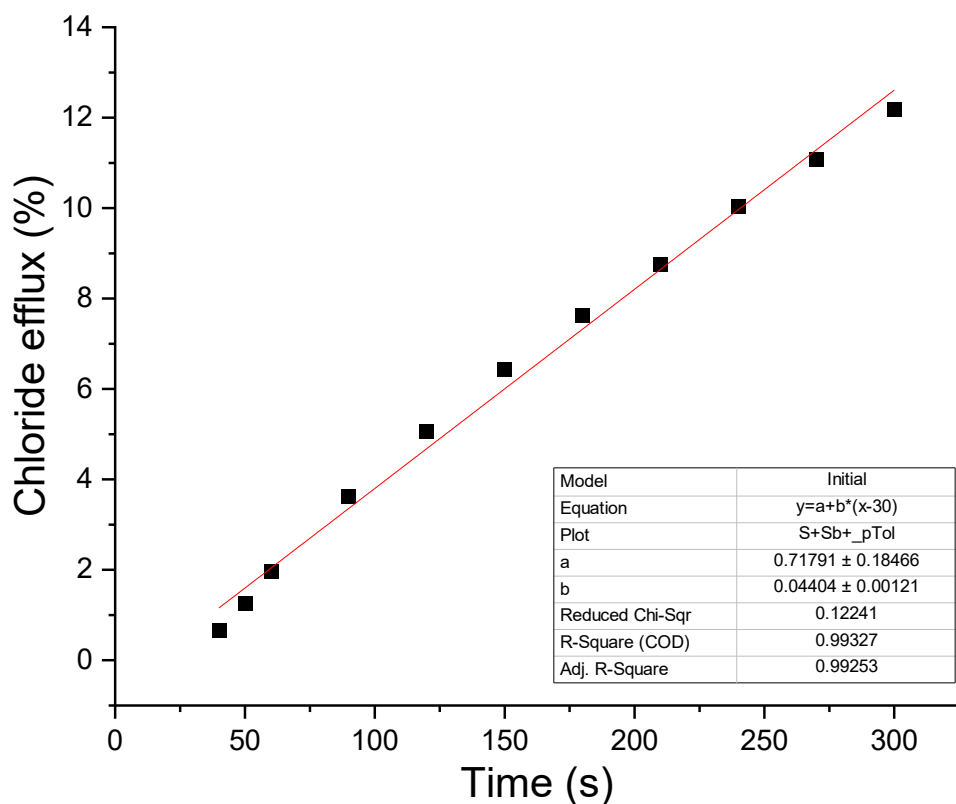


Figure S36. Kinetic fit of the valinomycin-coupled chloride efflux data observed when POPC vesicles are treated with $[4]^{2+}$ as a transporter (2.0 mol% with respect to the lipid concentration). The POPC vesicles were loaded with KCl (300 mM) and suspended in KGlc (300 mM) buffered to pH 7.2. Each data point represents the average of three repeat measurements. $k_{ini.} = b = 0.04 \text{ \%}\cdot\text{s}^{-1}$.

Hill plot measurements and analysis

The assay described in Figure S33 was carried out with different concentrations of stibonium cation ($[1]^+$ and $[2]^+$). The resulting data was used to generate Hill plots according to the following equation:

$$y = 100 \frac{x^n}{k^n + x^n}$$

where

x is the stibonium cation concentration

y is the chloride efflux (%) at 270 s

n is the Hill coefficient

k is the EC_{50} .

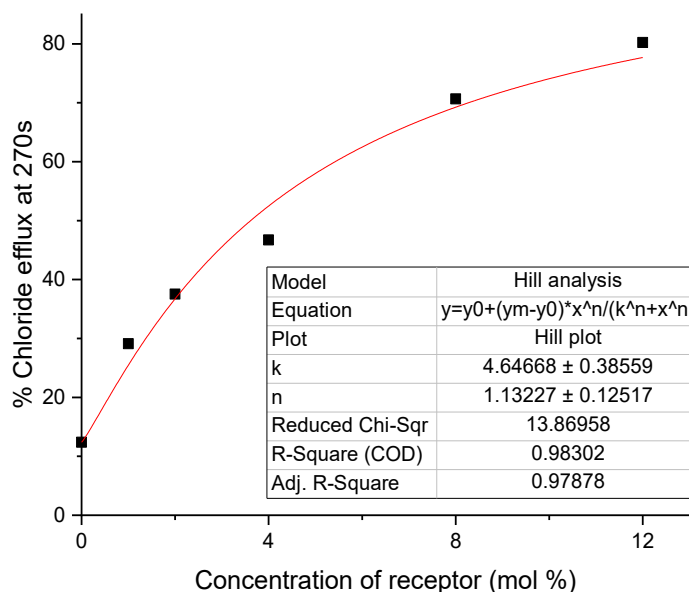
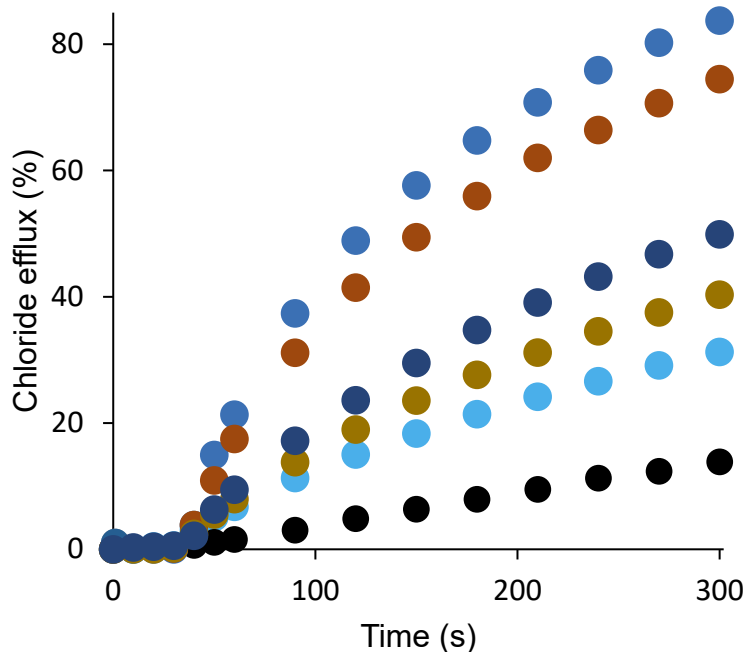


Figure S37. Hill plot analysis of the chloride efflux from POPC vesicles (POPC concentration = 0.7 mM) mediated by $[1]^+$ in the presence of valinomycin. Valinomycin (0.1 mol% with respect to the lipid concentration) was added at time $t = 0$ s as a DMSO solution. After the 30 s, the transporter ($[1]^+$) was added as a DMSO solution, and the chloride efflux was monitored using a chloride selective electrode. At $t = 300$ s, 50 μ L of a Triton X solution (10:1:0.1 H₂O:DMSO:Triton X (v/v/v)) was added to lyse the vesicles triggering complete release of the chloride cargo. The value corresponding to 100% chloride efflux was recorded at $t = 420$ s, 2 min. after lysing the vesicles. Concentrations of $[1]^+$ used: 0 mol% (DMSO), 1 mol%, 2 mol%, 4 mol%, 8 mol%, 12 mol% with respect to the lipid concentration. ($EC_{50} = 4.65 (\pm 0.39)$ mol%, $n = 1.13$).

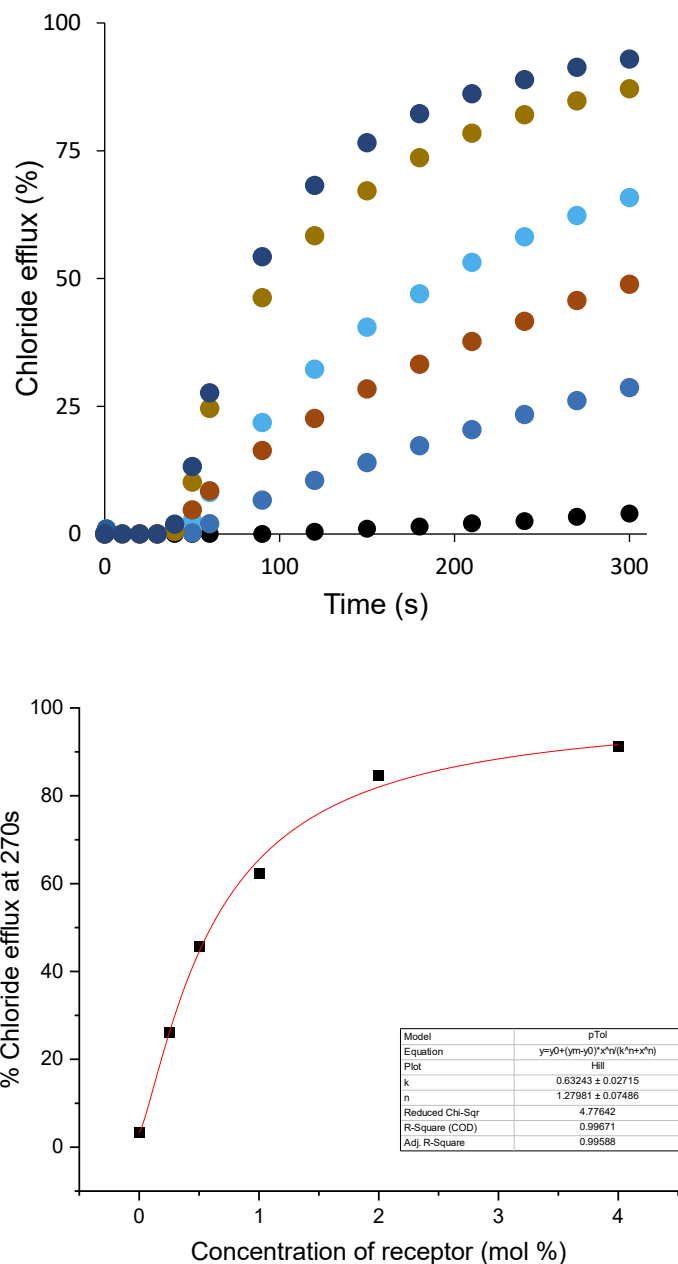


Figure S38. Hill plot analysis of the chloride efflux from POPC vesicles (POPC concentration = 0.7 mM) mediated by $[2]^+$ in the presence of valinomycin. Valinomycin (0.1 mol% with respect to the lipid concentration) was added at time $t = 0$ s as a DMSO solution. After the 30 s, the transporter ($[2]^+$) was added as a DMSO solution, and the chloride efflux was monitored using a chloride selective electrode. At $t = 300$ s, 50 μ L of a Triton X solution (10:1:0.1 H₂O:DMSO:Triton X (v/v/v)) was added to lyse the vesicles triggering complete release of the chloride cargo. The value corresponding to 100% chloride efflux was recorded at $t = 420$ s, 2 min. after lysing the vesicles. Concentrations of $[2]^+$ used: 0 mol% (DMSO), 0.25 mol%, 0.5 mol%, 1 mol%, 2 mol%, 4 mol% with respect to the lipid concentration. ($EC_{50} = 0.63(\pm 0.03)$ mol%, $n = 1.28(\pm 0.07)$).

Temperature-dependent chloride transport experiments in the presence of valinomycin using DPPC vesicles

Internal solution: KCl 300 mM, HEPES 10 mM, pH 7.2

External solution: KGlc 300 mM, HEPES 10mM, pH 7.2

DPPC vesicles containing KCl were suspended in the external solution (5 mL) at 25 °C or 45 °C such that the final lipid concentration was equal to 0.7 mM. After the signal of the voltage had stabilized (~30 s), the measurement was initiated using a chloride selective electrode at 25 °C or 45 °C. At $t = 0$ s, valinomycin dissolved in DMSO (0.7 mM) was added to the assay such that the final valinomycin concentration was 0.1 mol %. At $t = 30$ s, the stibonium cation ($[2]^+$) was added to the assay. At $t = 300$ s, 50 μ L of a Triton X solution (10:1:0.1 H₂O:DMSO:Triton X (v/v/v)) was added to lyse the vesicles triggering complete release of the chloride cargo. The value corresponding to 100% chloride efflux was recorded at $t = 420$ s, 2 min. after lysing the vesicles.

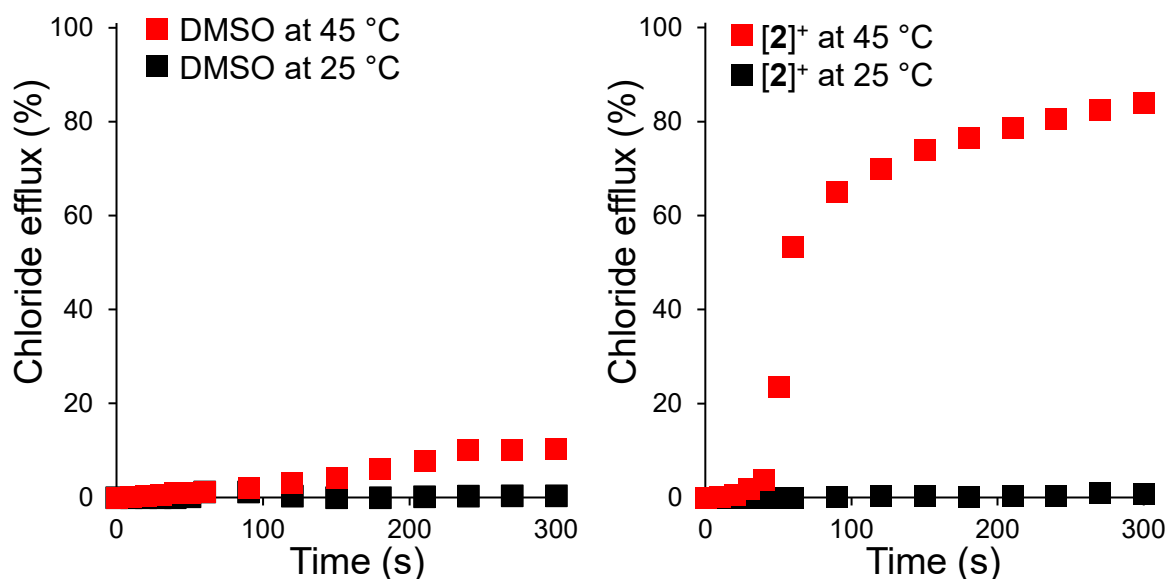


Figure S39. Temperature-dependent transport experiments carried out with DMSO and $[2]^+$ in DPPC-based vesicles.

Carboxylfluorescein (CF) non-specific leakage assay

Internal solution: KCl 10 mM, HEPES 10 mM, 50 mM CF, pH 7.4

External solution: KCl 100 mM, HEPES 10 mM, pH 7.4

POPC vesicles containing 50 mM CF were suspended in the external solution (3 mL) such that the final lipid concentration was equal to 0.1 mM. After the electrode voltage had stabilized (~30 s), the time dependent changes in fluorescence intensity ($\lambda_{\text{ex}} = 492 \text{ nm}$, $\lambda_{\text{em}} = 517 \text{ nm}$) was recorded. At $t = 50 \text{ s}$, the stibonium cation ($[2]^+$ or $[4]^{2+}$ with GSH) was added to the assay. At $t = 350 \text{ s}$, 50 mL of a Triton X solution (10:1:0.1 H₂O:DMSO:TritonX (v/v/v)) was added to lyse the vesicles triggering complete release of the vesicle membrane. The value $I_f = 1.0$ was recorded at $t = 420 \text{ s}$, 2 m after lysing the vesicles. The resulting data was used to obtain non-specific leakage plots according to the following equation:¹⁸

$$I_f = (I_t - I_0)/(I_\infty - I_0)$$

where

I_f is the changes in fluorescence intensity ($\lambda_{\text{ex}} = 492 \text{ nm}$, $\lambda_{\text{em}} = 517 \text{ nm}$).

I_t is the fluorescence intensity at t time.

I_0 is the fluorescence intensity right before the transporter addition

I_∞ is the fluorescence intensity after lysis.

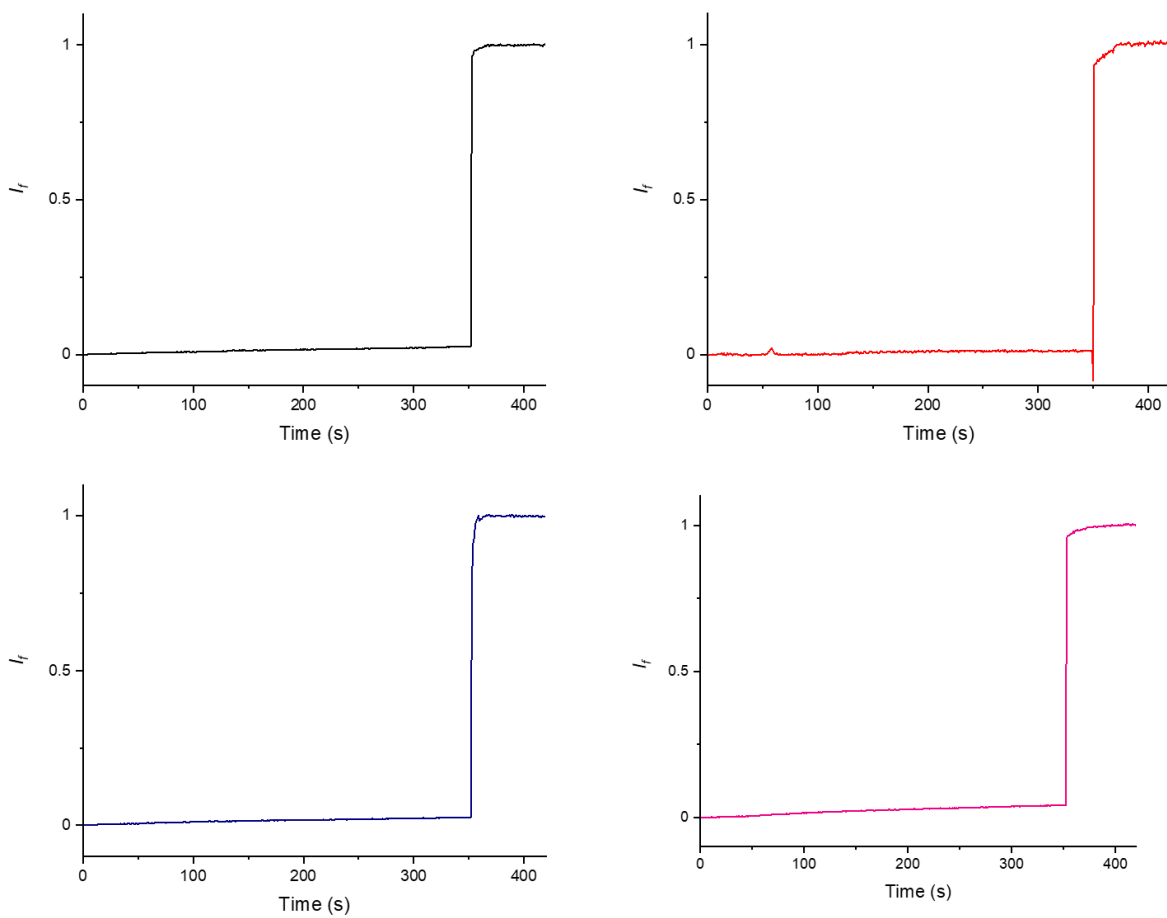


Figure S40. CF non-specific leakage for DMSO (top left), $[2]^+$ (top right), 6 equiv. GSH (bottom left) and 6 equiv. GSH+ $[4]^{2+}$ (bottom right). Fluorescence intensity was monitored after the addition of the transporters at EC_{50} concentration of $[2]^+$ at $t = 50$ s. Triton X-100 was added at $t = 350$ s.

Reduction of $[4]^{2+}$ by DMSO or by GSH

$[4]^{2+}$ (0.0035 mmol) was dissolved in $\text{DMSO-}d_6$ (0.7 mL) and its stability was monitored by ^1H NMR spectroscopy over the course of 5 h. As shown in Figure S41, $[4]^{2+}$ underwent almost complete reduction into $[2]^+$ over this period of time. The same general protocol was used to study the GSH mediated reduction described in the main text. In this case, GSH was dissolved in degassed D_2O to afford a stock solution with $[\text{GSH}] = 175 \text{ mM}$. An aliquot of this solution (60 μL) was added to the NMR tube containing the $\text{DMSO-}d_6$ solution of $[4]^{2+}$. The reaction was then monitored by ^1H NMR.

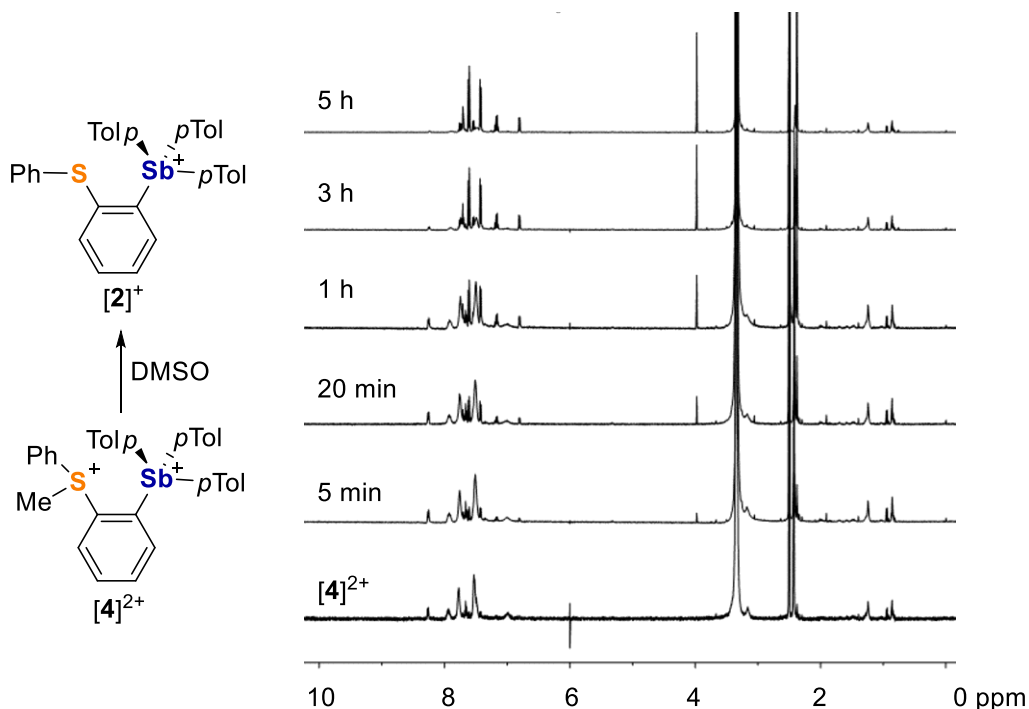


Figure S41. Spontaneous reduction of $[4]^{2+}$ in $\text{DMSO-}d_6$ monitored over time by ^1H NMR spectroscopy. The signal at 3.98 ppm is assigned to the formation of $[\text{O}=\text{SMe}(\text{CD}_3)_2]^+$.²⁰

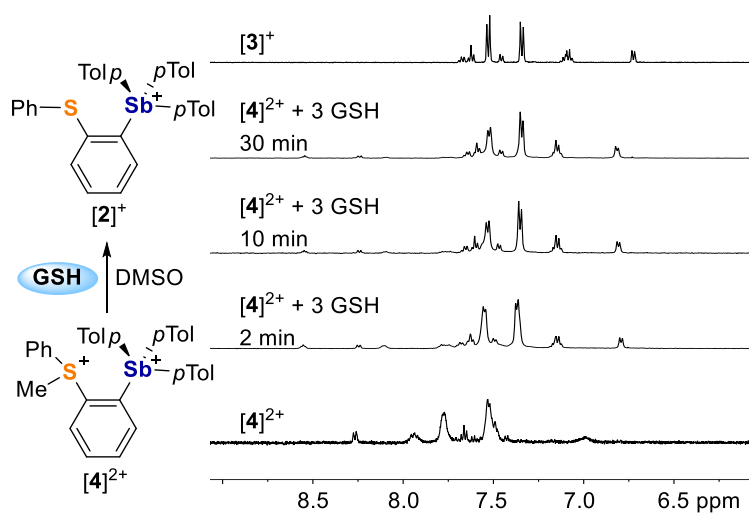


Figure S42. Reduction of $[\mathbf{4}]^{2+}$ (5 mM) by GSH (3 equiv.) in $\text{DMSO-}d_6$ monitored over time by ^1H NMR spectroscopy.

Reduction of $[4]^{2+}$ by GSH in DMSO:D₂O phosphate buffer (0.3 M, pH 7.6, v/v = 2.1:7.9)

$[4]^{2+}$ (0.007 mmol) was dissolved in DMSO-*d*₆ (0.3 mL) and D₂O (0.3 M phosphate buffer, pH 7.6, 1 mL). Monitoring of this mixture 90 min showed no reaction. The same general protocol was used to study the GSH mediated reduction described in the main text. In this case, GSH was dissolved in degassed D₂O to afford a stock solution with [GSH] = 175 mM. An aliquot of this solution (120 μL) was added to the NMR tube containing the DMSO-*d*₆/D₂O phosphate buffer solution of $[4]^{2+}$. Monitoring the ensuing reaction by ¹H NMR spectroscopy showed reduction of $[4]^{2+}$ into $[2]^+$ over the course of 90 min as illustrated in Figure 6 of the main text.

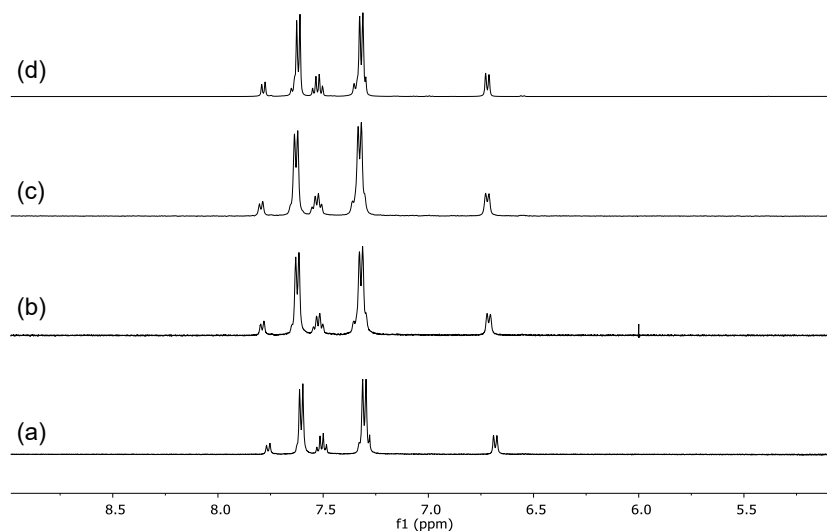


Figure S43. ¹H NMR spectra of (a) $[4]^{2+}$ in DMSO-*d*₆/D₂O phosphate buffer solutions after 0 min (a), 15 min (b), 45 min (c) and 90 min (d).

In situ activation of the preanionophore [4]²⁺ in the presences of chloride-loaded vesicles

Internal solution: KCl 300 mM, HEPES 10 mM, pH 7.4

External solution: KGlc 300 mM, HEPES 10 mM, pH 7.4

POPC vesicles containing KCl were suspended in the external solution (5 mL) such that the final lipid concentration was equal to 0.7 mM. GSH was delivered to this assay as an aqueous solution. [4]²⁺, dissolved in DMSO, was added to the vesicle solution such that the final concentration in [4]²⁺ was 2 mol%. The suspension was incubated at 37 °C for 20 min. The electrode was then immersed. After the electrode voltage had stabilized (~ 60s), the voltage recording was initiated (t = 0 s). At t = 10s, valinomycin dissolved in DMSO (0.7 mM) was added the assay such that the final valinomycin concentration was 0.1 mol%. At t = 300s, 50 µL of a Triton X solution (10:1:0.1 H₂O:DMSO:Triton X (v/v/v)) was added to lyse the vesicles triggering complete release of the chloride cargo. The value corresponding to 100% chloride efflux was recorded at t = 420s, 2 min. after lysing the vesicles. This experiment was carried with the following GSH concentrations: 25 µM, 50 µM and 100 µM.

References

1. J. Vicente, J. A. Abad and R. M. López-Nicolás, *Tetrahedron*, 2008, **64**, 6281-6288.
2. A. P. M. Robertson, S. S. Chitnis, H. A. Jenkins, R. McDonald, M. J. Ferguson and N. Burford, *Chem. Eur. J.*, 2015, **21**, 7902-7913.
3. N. Bricklebank, S. M. Godfrey, H. P. Lane, C. A. McAuliffe and R. G. Pritchard, *J. Chem. Soc., Dalton Trans.*, 1994, DOI: 10.1039/DT9940001759, 1759-1763.
4. K. H. Chan, W. K. Leong and K. H. G. Mak, *Organometallics*, 2006, **25**, 250-259.
5. M. J. Frisch, G. W. Trucks, H. B. Schlegel, G. E. Scuseria, M. A. Robb, J. R. Cheeseman, G. Scalmani, V. Barone, B. Mennucci, G. A. Petersson, H. Nakatsuji, M. Caricato, X. Li, H. P. Hratchian, A. F. Izmaylov, J. Bloino, G. Zheng, J. L. Sonnenberg, M. Hada, M. Ehara, K. Toyota, R. Fukuda, J. Hasegawa, M. Ishida, T. Nakajima, Y. Honda, O. Kitao, H. Nakai, T. Vreven, J. Montgomery, J. A.; , J. E. Peralta, F. Ogliaro, M. Bearpark, J. J. Heyd, E. Brothers, K. N. Kudin, V. N. Staroverov, R. Kobayashi, J. Normand, K. Raghavachari, A. Rendell, J. C. Burant, S. S. Iyengar, J. Tomasi, M. Cossi, N. Rega, J. M. Millam, M. Klene, J. E. Knox, J. B. Cross, V. Bakken, C. Adamo, J. Jaramillo, R. Gomperts, R. E. Stratmann, O. Yazyev, A. J. Austin, R. Cammi, C. Pomelli, J. W. Ochterski, R. L. Martin, K. Morokuma, V. G. Zakrzewski, G. A. Voth, P. Salvador, J. J. Dannenberg, S. Dapprich, A. D. Daniels, Ö. Farkas, J. B. Foresman, J. V. Ortiz, J. Cioslowski and D. J. Fox, *Gaussian 09*, Revision D.01, Gaussian, Inc., Wallingford, CT, 2013.
6. P. J. Stephens, F. J. Devlin, C. F. Chabalowski and M. J. Frisch, *J. Phys. Chem.*, 1994, **98**, 11623-11627.
7. A. D. Becke, *J. Chem. Phys.*, 1993, **98**, 5648-5652.
8. B. Metz, H. Stoll and M. Dolg, *J. Chem. Phys.*, 2000, **113**, 2563-2569.
9. M. D. Hanwell, D. E. Curtis, D. C. Lonie, T. Vandermeersch, E. Zurek and G. R. Hutchison, *J. Cheminformatics*, 2012, **4**, 17.
10. T. Lu and F. Chen, *J. Comput. Chem.*, 2012, **33**, 580-592.
11. W. Humphrey, A. Dalke and K. Schulten, *J. Mol. Graph.*, 1996, **14**, 33-38.
12. R. F. Ribeiro, A. V. Marenich, C. J. Cramer and D. G. Truhlar, *J. Phys. Chem. B*, 2011, **115**, 14556-14562.
13. M. Kolar, J. Fanfrlik, M. Lepsik, F. Forti, F. J. Luque and P. Hobza, *J. Phys. Chem. B*, 2013, **117**, 5950-5962.
14. A. V. Marenich, C. J. Cramer and D. G. Truhlar, *J. Phys. Chem. B*, 2009, **113**, 6378-6396.
15. F. Vlahovic, S. Ivanovic, M. Zlatar and M. Gruden, *J. Serb. Chem. Soc.*, 2017, **82**, 1369-1378.
16. H. J. Clarke, E. N. Howe, X. Wu, F. Sommer, M. Yano, M. E. Light, S. Kubik and P. A. Gale, *J. Am. Chem. Soc.*, 2016, **138**, 16515-16522.
17. A. Vargas Jentzsch, D. Emery, J. Mareda, S. K. Nayak, P. Metrangolo, G. Resnati, N. Sakai and S. Matile, *Nat. Commun.*, 2012, **3**, 905.
18. S. Benz, M. Macchione, Q. Veroleto, J. Mareda, N. Sakai and S. Matile, *J. Am. Chem. Soc.*, 2016, **138**, 9093-9096.
19. L. A. Jowett, E. N. W. Howe, X. Wu, N. Busschaert and P. A. Gale, *Chem. Eur. J.*, 2018, **24**, 10475-10487.

20. E. Avella-Moreno, N. Nuñez-Dallos, L. Garzón-Tovar and A. Duarte-Ruiz, *J. Sulfur Chem.*, 2015, **36**, 535-543.